Universidade de Aveiro
Ano 2022

MARTA BONIFÁCIO PINHO E COSTA

REGULAÇÃO DO CANAL DE MAGNÉSIO MGTE POR DI-AMP CÍCLICO

REGULATION OF THE MAGNESIUM CHANNEL MGTE BY CYCLIC-DI-AMP

Universidade de Aveiro
Ano 2022

MARTA BONIFÁCIO PINHO E COSTA

REGULAÇÃO DO CANAL DE MAGNÉSIO MGTE POR DI-AMP CÍCLICO

REGULATION OF THE MAGNESIUM CHANNEL MGTE BY CYCLIC-DI-AMP

Dissertação apresentada à Universidade de Aveiro para cumprimento dos requisitos necessários à obtenção do grau de Mestre em Biologia Aplicada, realizada sob a orientação científica da Doutora Angela Cunha, Professora Auxiliar com Agregação do Departamento de Biologia e CESAM da Universidade de Aveiro e do Doutor João Morais Cabral, Investigador Principal do IBMC - i3s da Universidade do Porto.

It's the job that's never started as takes longest to finish.

— J.R.R. Tolkien

o júri

Presidente	Professora Doutora Etelvina Maria de Almeida Paula Figueira Professora Auxiliar, Departamento de Biologia, Universidade de Aveiro
Vogal – Arguente	Professor Doutor Brian James Goodfellow Professor Auxiliar, Departamento de Química, Universidade de Aveiro
Vogal – Coorientador	Doutor João Henrique Resende de Oliveira Morais Cabral Investigador Principal, i3S – Instituto de Investigação e Inovação em Saúde, Universidade do Porto

agradecimentos

Agradeço, antes de mais, a todos os que me apoiaram e suportaram durante o último ano:

João Morais Cabral, por me ter dado esta oportunidade, e por todo o seu apoio, confiança e disponibilidade. Ensinou-me mais que alguma vez esperei ser possível.

Angela Cunha, por ter aceitado a nossa proposta e pela imensa paciência e disponibilidade que me mostrou.

Ao grupo Structural Biochemistry, Carol Harley, Katharina Weinhaeupl, Andreia Fernandes e Tatiana Cereija por me terem acolhido e porporcionado constante ajuda e aprendizagem. A Inês Rosa Costa, pela companhia e amizade durante ambos os nossos percursos.

Aos meus amigos, por me terem empurrado, ouvido vez e vez sem conta, e estarem sempre lá quando precidei, mesmo com os seus muito maiores problemas. Matilde, Miguel, muito obrigada.

E à minha família, que não precisava de ter tido a benevolência que teve. À minha Mãe, sem quem nunca terei voltado a este mestrado, ao meu Pai, sempre disposto a ajudar-me, ao meu Tio, pelo seu comentário sempre perspicaz. E ao Gabriel, com quem sempre pude ser honesto e quem percebe, percebe.

palavras-chave

Magnésio, c-di-AMP, MgtE, canal iónico, domínio CBS.

resumo

As células são sistemas complexos e adaptáveis que mantêm um controlo apertado sobre os gradientes de concentração de iões inorgânicos como K^+, Na^+, Cl^-, Ca^{2+} e Mg^{2+}, vitais para uma série de funções celulares como a regulação de pH, o controlo de osmolaridade, a actividade eléctrica, e a comunicação celular. Para este fim, as células possuem uma variedade de transportadores e canais que facilitam a sua passagem através da membrana celular.

O magnésio (Mg^{2+}) é o segundo catião intracelular mais abundante, um importante cofactor enzimático, componente estrutural, e estabilizador do ADN. Em Bacteria, vários canais e transportadores regulam o influxo e efluxo de Mg^{2+}, incluindo o canal MgtE. O MgtE possui um domínio de cistathionine-β-synthase, o domínio CBS, que pode ligar ligandos contendo adenosina, com funções reguladoras noutros transportadores. Entre esses ligandos, encontramos o di-AMP cíclico um mensageiro segundário de nucleótido cíclico que modula o transporte de K^+ a vários níveis e que foi proposto ligar-se ao MgtE. Recentemente, foram observadas alterações nas concentrações intracelulares de Mg^{2+}, K^+ e di-AMP cíclico durante a resposta ao stress osmótico. O principal objectivo deste trabalho é provar que o di-AMP cíclico se liga ao MgtE de *B. subtilis*, uma bactéria Gram-positiva modelo, e explorar os seus efeitos no transporte de Mg^{2+} através do MgtE.

Neste trabalho, foram realizados ensaios funcionais, confirmando o que o MgtE é um canal de Mg^{2+}, mas não foram obtidos resultados conclusivos sobre os efeitos do di-AMP cíclico. Foram realizadas a expressão e purificação em grande escala do domínio N-terminal do MgtE (contendo o sub-domínio CBS), seguidos de ensaios estruturais. Os ensaios de fluorimetria de varrimento diferencial identificaram o di-AMP cíclico como um ligando, e a calorimetria isotérmica de titulação determinou que a ligação ocorre com uma constante de dissociação K_D de 1,75 μM e uma estequiometria de 1:4 moléculas de di-AMP cíclico para moléculas de MgtE. A cromatografia de exclusão de tamanho revelou que o domínio citosólico do MgtE sofre uma alteração conformacional, apoiando a oligomerização do domínio na presença do di-AMP cíclico. Finalmente, os ensaios de cristalografia produziram vários cristais para análise, mas a estrutura do complexo proteína-ligando não pôde ser resolvida devido à má qualidade dos cristais.

keywords Magnesium, c-di-AMP, MgtE, ion channel, CBS domain

abstract

Cells are complex, adaptable systems that maintain a tight control over the concentration gradients of inorganic ions like K^+, Na^+, Cl^-, Ca^{2+} and Mg^{2+}, vital for a host of cellular functions like pH regulation, osmolarity control, electrical activity, and cellular communication. For this purpose, cells possess a variety of transporters and channels that facilitate their passage through the cell membrane.

Magnesium (Mg^{2+}) is the second most abundant intracellular cation, an important enzyme cofactor, structural component, and stabilizer of DNA. In Bacteria, several channels and transporters regulate Mg^{2+} influx and efflux, including the MgtE channel. MgtE possesses a cystathionine-β-synthase domain, the CBS domain, that can bind adenosine-containing ligands, with regulatory functions in other transporters. Among such ligands, we find cyclic-di-AMP, a cyclic nucleotide second messenger that modulates K^+ transport at several levels and has been proposed to bind to MgtE. Recently, changes in intracellular Mg^{2+}, K^+ and cyclic-di-AMP concentrations were observed during osmotic stress response. The main goal of this work is to prove that cyclic-di-AMP binds to MgtE from *B. subtilis*, a model Gram-position bacteria, and to explore its effects on Mg^{2+} transport through MgtE.

In this work, functional assays were performed, confirming MgtE's role as a Mg^{2+} channel, but no conclusive results about cyclic-di-AMP's effects were obtained. Large-scale expression and purification of MgtE's N-terminal domain (containing the CBS sub-domain) were performed, followed by structural assays. Differential scanning fluorimetry assays identified cyclic-di-AMP as a ligand, and isothermal titration calorimetry determined that binding occurs with a dissociation constant K_D of 1.75 μM and a stoichiometry of 1:4 cyclic-di-AMP to MgtE molecules. Size-exclusion chromatography revealed that MgtE's cytosolic domain undergoes a conformational change, supporting the oligomerization of the domain in the presence of cyclic-di-AMP. Finally, crystallography assays yielded several crystals for analysis, but the structure of the protein-ligand complex could not be resolved due to poor crystal quality.

TABLE OF CONTENTS

LIST OF FIGURES

LIST OF TABLES

LIST OF SCHEMES

LIST OF ABBREVIATIONS

$(NH_4)_2SO_4$	Ammonium sulfate
Å	Ångström
AMP	Adenosine monophosphate
ATP	Adenosine triphosphate
ATPase	Adenosine triphosphatase
Ca^{2+}	Calcium ion
$CaCl_2$	Calcium chloride
CBS	Cystathionine-β-synthase
c-di-AMP	Cyclic di-adenosine monophosphate
c-di-GMP	Cyclic di-guanosine monophosphate
Cl^-	Chloride ion
Co^{2+}	Cobalt ion
CV	Column volume
cyclic GMP-AMP	Cyclic guanosine monophosphate adenosine monophosphate
cyclic-AMP	Cyclic adenosine monophosphate
cyclic-di-AMP	Cyclic di-adenosine monophosphate
cyclic-di-GMP	Cyclic di-guanosine monophosphate
Da	Dalton
DAC	Diadenylyl cyclase
DMSO	Dimethyl sulfoxide
DNA	Desoxyribonucleic acid
DRaCALA	Differential Radial Capillary Action of Ligand Assay
DSF	Differential scanning fluorimetry
$FeCl_3$	Iron(III) chloride
$FeSO_4$	Iron(II) sulfate
H^+	Hydrogen ion / Proton
HCl	Hydrogen chloride
HEPES	4-(2-hydroxyethyl)-1-piperazineethanesulfonic acid
His-tag	Hexahistidine tag
IPTG	Isopropylthio-β-galactoside
ITC	Isothermal titration calorimetry
K^+	Potassium ion
K_2HPO_4	Dipotassium phosphate
KA	Association constant
kcal	Kilocalorie
KCl	Potassium chloride
KD	Dissociation constant
KH_2PO_4	Monopotassium phosphate
LB	Lysogeny broth

LB20Mg	LB with 20mm Mg^{2+}
LB30Mg	LB with 30mm Mg^{2+}
mg	Milligram
Mg^{2+}	Magnesium ion
$MgCl_2$	Magnesium chloride
$MgSO_4$	Magnesium sulfate
mL	Milliliter
mM	Millimolar
MOPS	3-(N-morpholino)propanesulfonic acid
Na	Sodium
Na^+	Sodium ion
Na_2HPO_4	Disodium phosphate
NaCl	Sodium chloride
NaH_2PO_4	Monosodium phosphate
nm	Nanometer
OD	Optical density
OD_{600nm}	Optical density at a wavelength of 600 nanometers
pApA	5'- Phosphoadenylyl- (3' → 5')- adenosine
PCR	Polymerase chain reaction
PEG	Polyethylene glycol
pH	Power of hydrogen
PMSF	Phenylmethylsulfonyl fluoride
ppgpp	Guanosine tetraphosphate
pppgpp	Guanosine pentaphosphate
RCK	Regulating the conductance of K^+
RFU	Linear 5'-phosphadenylyl-adenosine
rpm	Revolutions per minute
SD	Standard deviation
SDS-PAGE	Sodium dodecyl sulfate polyacrylamide gel electrophoresis
STING	Stimulator of interferon genes
T_m	Melting temperature
Tm	Melting temperature
TrisHCL	Trisaminomethane hydrochloride
ΔH	Binding enthalpy
ΔT_m	Thermal shift
µg	Microliter
µg	Microgram
µM	Micromolar

1. INTRODUCTION

1.1. Magnesium, essential to life

All cells accumulate or extrude inorganic ions (K^+, Na^+, Cl^-, Ca^{2+}, Mg^{2+}), generating concentration gradients that are used for many cellular functions including, electrical activity, regulation of internal pressure and pH and cellular communication. As seen in Figure 1, of the ions necessary to the survival of life, magnesium is the second most abundant inside the cell, just after potassium, and the most abundant divalent cation. Within cells, it is found in total concentrations of 5-30 mM (Hartwig, 2001), with free Mg^{2+} concentrations of 0.5-1 mM in the cytoplasm (Began *et al.*, 2020).

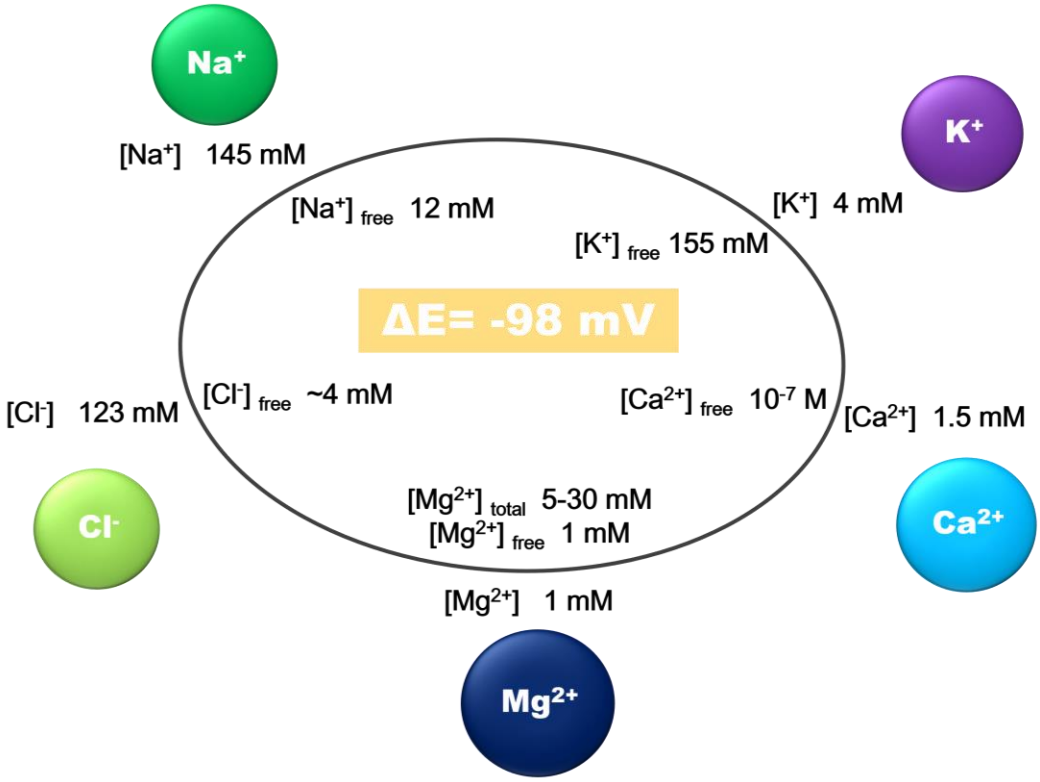

Figure 1– Mammalian skeletal muscle cell depicting the concentration gradient of inorganic ions necessary to the survival of life, and the cell resting membrane potential, largely derived from this electrochemical gradient.

Magnesium ions play several essential roles in cells, as a cofactor for enzyme activity, a structural component of the ribosome, but also an element necessary for genomic and membrane stability (Moncrief and Maguire, 1999; Hartwig, 2001; Moomaw and Maguire, 2008). As consequence, Mg^{2+} deficiency is linked to severe diseases including cardiac syndromes, muscular dysfunction and bone wasting (Rude, 1998; de Baaij, Hoenderop and Bindels, 2015; DiNicolantonio, O'Keefe and Wilson, 2018).

It is important to note that the magnesium cation possesses several attributes that make it unique. Its hydrated radius is the largest of all biological cations, but its ionic

radius is among the smallest's. It translates to a hydrated volume over 400x greater than its dehydrated volume. It is also strictly hexacoordinate and its coordination sphere is much more rigid compared to other ions like Ca^{2+}. (Maguire and Cowan, 2002).

Such physico-chemical properties raise specific challenges when considering binding sites in transport proteins and their mechanism of transport. The volume changes between the hydrated and dehydrated forms of the ion alone pose a potential problem for magnesium transport proteins, because they need to remove the hydration shell to carry the bare ion through the transmembrane pathways (Moncrief and Maguire, 1999; Maguire and Cowan, 2002).

1.2. Mg^{2+} Transporters in Bacteria

When it comes to the transport of magnesium through the cell membrane, four families of transport proteins have been discovered in bacteria (Table 1) (Franken *et al.*, 2022; Jin, Huang and Hattori, 2022)

Table 1– Overview of prokaryotic Mg2+ transporter superfamilies.

Prokaryotic superfamilies	Transport mechanism	Eukaryotic orthologues
CorA	Channel	Mrs2, Lpe10
MgtE	Channel	SLC41
MgtA	P-type ATPase	—
CorC	Exchanger (?)	CNNM

The MgtE family, a primary magnesium channel, is found throughout prokaryotic phyla, in Bacteria as well as Archaea (Groisman *et al.*, 2013). Interestingly, its eukaryotic ortholog SLC41 appears to function as a Mg^{2+}/Na^{+} antiporter (Jin, Huang and Hattori, 2022), suggesting that these proteins utilize different molecular mechanism within a similar structural fold and similar function. Similarly, the CorA family is a primary magnesium channel with wide distribution across phylogenetic branches (Groisman *et al.*, 2013). The MgtA family, however, is composed of active Mg^{2+} transporters. These P-type ATPases are only found in certain bacteria and expressed when in low Mg^{2+} concentrations (Groisman *et al.*, 2013). Finally, the CorC family has only recently been studied in more detail and is thought to function as a transporter driven by the Na^{+} gradient (Jin, Huang and Hattori, 2022).

1.2.1. The MgtE channel

MgtE carries Mg^{2+} across the cell membrane down the electrochemical gradient (Groisman *et al.*, 2013) and is highly selective for Mg^{2+} (Hattori *et al.*, 2009). As Hattori *et al.* first elucidated in 2007, then further developed in 2009, MgtE arranges itself as a homodimer. Depicted in Figure 2, it has a C-terminal transmembrane domain and an N-terminal cytosolic domain. The transmembrane domain of each subunit is composed by five helices, for a total of ten per channel. These helices form the ion conducting pore

through which Mg^{2+} travels. The cytosolic domain is subdivided into two components: the N-terminal domain and a tandem repeat of cystathionine-β-synthase (CBS) domains. It is important to note here that CBS domains have regulatory functions and channel gating functions, and are binding targets for ligands such as ATP and AMP (Ignoul and Eggermont, 2005; Gundlach *et al.*, 2019). In MgtE, the CBS and transmembrane domains are connected by a helix, known as the "connecting" or "plug" helix (Jin, Huang and Hattori, 2022).

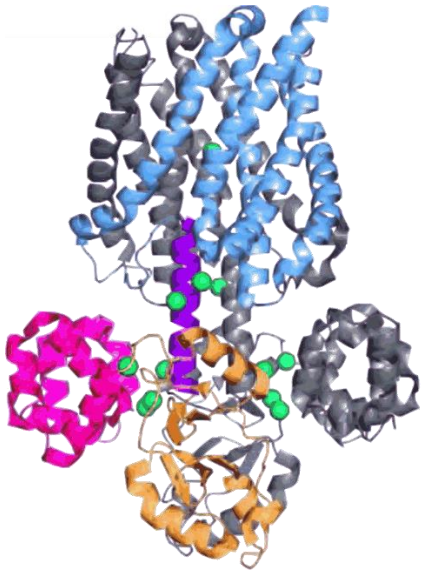

Figure 2– Cartoon representation of full-length MgtE from *T. thermophilus* (PDB ID: 2ZY9).
One protomer is shown with the N-terminal domain in pink, the CBS domains in orange, the connecting helix in purple and the C-terminal transmembrane domain in blue. Another protomer appears in gray. Mg^{2+} ions are colored in green. Adapted from Jin, Huang and Hattori, 2022.

In *B. subtilis*, *mgtE* expression is controlled by the M-BOX, a magnesium-sensing riboswitch. (Hattori *et al.*, 2009) MgtE activity is also directly controlled by the intracellular Mg^{2+}. The cytosolic domain of MgtE possesses several Mg^{2+} binding sites. The presence or absence of Mg^{2+} induces conformational changes, with high concentrations of magnesium cation stabilizing the cytosolic domains and their connections with the transmembrane domains, leading the plug helices to close the ion-conducting pore, whereas it remains flexible and potentially open to Mg^{2+} transport at low concentrations of Mg^{2+} (Jin, Huang and Hattori, 2022). ATP further modulates the capability of MgtE to sense Mg^{2+} and regulate itself. When ATP is bound to MgtE, its CBS domain, affinity for Mg^{2+} increases, lowering the inactivation threshold into the range of free intracellular Mg^{2+}. (Tomita *et al.*, 2017)

Interestingly, it has been shown through Differential Radial Capillary Action of Ligand Assay (DRaCALA) that the MgtE channel from *B. subtilis* binds the second-messenger c-di-AMP, suggesting that this dinucleotide regulates the major Mg^{2+} transport protein in this organism (Gundlach *et al.*, 2019).

1.3. Cyclic-di-AMP, the secondary messenger

The physiological function of proteins, including Mg^{2+} channels and transporters, is strongly determined by their mechanisms of regulation. In particular by the signals (physical or chemical) that elicit changes in their activity levels.

In cells, intracellular concentration of secondary messengers rises or decreases in response to intra- or extra-cellular stimuli that promote production or degradation of the messenger molecule. The second messenger binds to regulatory domains, inducing conformational changes that alter the function of effector domains, eliciting a cellular response. Thus, secondary messenger signaling is one of the cellular processes used to reach an appropriate and adjusted response to stimuli. In bacteria, second messengers are most often nucleotide-based molecules, such as cyclic-AMP, cyclic-di-GMP, and more recently discovered, cyclic GMP-AMP. Within the same family, we find cyclic-di-AMP (Figure 3) (Yin *et al.*, 2020).

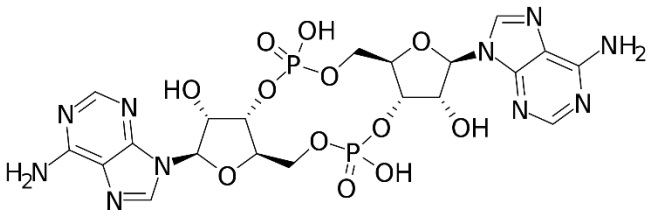

Figure 3– Cyclic di-AMP

Cyclic di-adenosine monophosphate (c-di-AMP) is product of diadenylyl cyclase activity from a DAC domain, where two ATP molecules are condensed to form c-di-AMP. This nucleotide is widely distributed in prokaryotes and found in most gram-positive bacteria, but not in eukaryotes, where its presence in cells unleashes an immune reaction. In mammals, STING recognizes c-di-AMP and triggers a type I interferon response. (Burdette *et al.*, 2011; Mudgal *et al.*, 2021)

c-di-AMP is conditionally essential for many bacteria, including in the model organism *B. subtilis*, being required for survival when growth occurs in complex media. It is also toxic at high levels: accumulation of c-di-AMP results in greater stress sensitivity and defects in cell division, (Mehne *et al.*, 2013; Stülke and Krüger, 2020) making it a messenger of primary importance in the study of prokaryotes, pathogenic or not.

This signaling molecule is also known for regulating processes at different stages, binding to riboswitches to regulate transcription, and binding directly to proteins to modulate their activity. In particular, c-di-AMP regulates a significant number of proteins that contain RCK (regulating conductance of K^+) or CBS (cystathionine-β-synthase) domains. (Stülke and Krüger, 2020)

c-di-AMP regulates and modulates a variety of functions including DNA damage repair, cell wall structure, metabolic activity and osmoregulation (Corrigan *et al.*, 2011; Cereija *et al.*, 2021). It binds to transporter proteins involved in osmoregulation such as OpuC and OpuA. It also has been proposed to be involved in the regulation of the K^+ machinery (Figure 4). It is thought to inactivate the K^+ importers KupA, KupB, KimA and KtrCD while also affecting the transcription of KimA and KtrAB by interacting with their riboswitches,

and of KdpFABC by binding to the sensor kinase in a two-component sensor that controls KdpFABC transcription (Yin *et al.*, 2020; Mudgal *et al.*, 2021). In contrast, c-di-AMP has been shown to activate the K^+ exporter KhtTU, as shown by the group where I have performed my Master research project (Cereija *et al.*, 2021) and has been proposed to modulate the activity of CpaA, another K^+ exporter (Corrigan and Gründling, 2013).

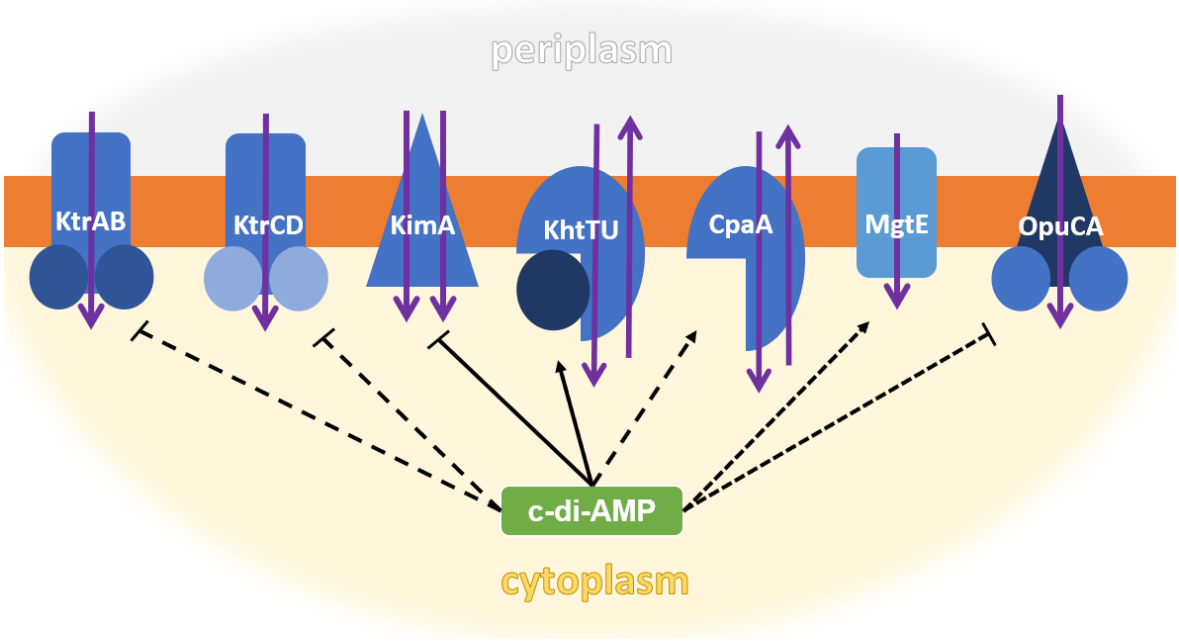

Figure 4– Schematic representation of transporters in *B. subtilis* regulated by c-di-AMP.
Black lines and black dotted lines represent known and proposed, respectively, c-di-AMP effects on proteins, with arrows representing positive regulation and bars representing negative regulation. Purple arrows represent movement of ions and solutes across the cell membrane, which is represented in orange.

Given the large number of potassium and osmolyte transporters controlled by c-di-AMP, it was proposed that this dinucleotide functions as a master regulator for K^+ homeostasis (Stülke and Krüger, 2020; Yin *et al.*, 2020; Cereija *et al.*, 2021). In this context, the regulation of the major Mg^{2+} transport protein, MgtE, in *B. subtilis*, raises questions about the physiological relationship between the intracellular levels of K^+ and Mg^{2+}. This potential relationship has been further revealed by a recent study that showed that upon hyperosmotic shock, *B. subtilis* cells uptake K^+ and release Mg^{2+} while the levels of intracellular c-di-AMP change to regulate the osmoprotectant cellular response (Wendel *et al.*, 2022).

1.4. Goals and Aims

In previous studies, it was proposed that c-di-AMP binds to MgtE, possibly at its CBS domain (Gundlach *et al.*, 2019; Stülke and Krüger, 2020). Heavily involved in K^+ machinery regulation, it was surprising to propose that c-di-AMP might be associated with the regulation of a Mg^{2+} channel. If c-di-AMP regulates MgtE, it would further widen c-di-AMP's already broad role in bacterial osmoregulation and ionic homeostasis (Cereija *et*

al., 2021). Thus, we believed it is of great interest to confirm and characterize c-di-AMP's binding to MgtE.

The primary goal of this work was to determine whether c-di-AMP binds to MgtE and how it modulates its function. The specific objectives were: 1) Does c-di-AMP bind to the CBS domain as proposed? 2) Does c-di-AMP have a role in Mg^{2+} transport through MgtE?

To achieve these objectives, we tested the functional properties of *B. subtilis*' MgtE and c-di-AMP using phenotype complementation assays, and the binding properties of the CBS domain of *B. subtilis*' MgtE using differential scanning fluorimetry, isothermal titration calorimetry, size-exclusion chromatography, protein crystallization and x-ray crystallography.

Ultimately, we would like to understand the implications of c-di-AMP regulation of intracellular levels of Mg^{2+} for bacterial survival and virulence.

2. METHODOLOGY

2.1. Bacterial strains and Growth media

Bacterial growth media were prepared as depicted in Table 2; sterilization was realized by autoclaving for 20 minutes at 121 °C. Information about the *E. coli* strains used during this work is displayed in Table 3.

Table 2– Composition of the growth media used throughout this work.

Lysogeny Broth (LB)	10 g/L Tryptone, 5 g/L Yeast Extract, 10 g/L NaCl
LB with 20mM Mg^{2+} (LB20Mg)	10 g/L Tryptone, 5 g/L Yeast Extract, 10 g/L NaCl, 20 mM $MgCl_2$
LB with 30mM Mg^{2+} (LB30Mg)	10 g/L Tryptone, 5 g/L Yeast Extract, 10 g/L NaCl, 30 mM $MgCl_2$
1mM [K^+] Minimal Media	8 mM $(NH_4)_2SO_4$, 400 µ M $MgSO_4$, 6 µ M $FeSO_4$, 6 µ M $FeCl_3$, 1mM Na citrate, 1 mg/L Thiamine HCl, 2 g/L Glucose, 10 mg/L $CaCl_2$, 400 µ M K_2HPO_4, 200 µM KH_2PO_4, 44.6 mM Na_2HPO_4, 22.8 mM NaH_2PO_4

Table 3– Genotype information of the *E. coli* strains used throughout this work.

BL21 (DE3)	F- ompT lon hsdSB (rB-mB-) gal dcm (DE3)
NEB 5-alpha	fhuA2 Δ(argF-lacZ) U169 phoA glnV44 Φ80 Δ(lacZ)M15 gyrA96 recA1 relA1 endA1 thi-1 hsdR17
TM2	[W3110] ΔmgtA ΔcorA yhiD::kan

2.2 Molecular Biology

DNA constructs were created using traditional molecular biology techniques. Sequence of *Bacillus subtilis* genomic DNA available through Subtiwiki (http://subtiwiki.uni-goettingen.de/) and sequences of used plasmids were analyzed for compatible restriction sites. Based on this analysis primers were designed (see Table 4).

Table 4– Primers and templates used to prepare the vectors used in the studies on MgtE.

Designation	Insert	Vector (Antibiotic resistance)	Primers
WT MgtE (pET24dNStrep_MgtE)	MgtE	pET24d-N-StrepTag-thrombin * (Kanamycin)	Forward: (**EcoRI**) 5′-GGAACCGAATTCGTTCAAAACATGACCTATG-3′ Reverse: (**XhoI**) 5′-GGAACC CTCGAGTTATAATGAGTGAATG-3′
MgtE CBS-L (pET24dT_CBSL)	CBS domain of	Pet24dT * (Kanamycin)	Forward: (**NcoI**) 5′-CCGTTCCCCATGGAAGTTCAAAACATGACC-3′

	MgtE		Reverse: (**XhoI**) 5′-GGAACCCTCGAGTTACCGGTATGCCGC-3′
MgtE CBS-S (pET24dT_CBSS)	CBS domain of MgtE	Pet24dT * (Kanamycin)	Forward: (**NcoI**) 5′-CCGTTCC CCATGGAAGTTCAAAACATGACC-3′ Reverse: (**XhoI**) 5′-GGAACC CTCGAGTTATTTTTCGTAATC-3′
MgtE (pBADHisB_MgtE)	MgtE	pBAD/HisB (Ampicillin)	Forward: (**PscI**) 5′-CCGTTCCACATGTCTGTTCAAAACATGACC-3′ Reverse: (**XhoI**) 5′-GGAACC CTCGAGTTATAATGAGTGAATG-3′

* pET24d-N-StrepTag and pet24dT are modifications of the commercially available pET24d; pET24d-N-StrepTag adds a Strep-tag and thrombin cleavage site at the N terminus of the expressed protein while pet24dT adds a thrombin cleavage site just before the His-tag of pet24d.

For assays aimed at studying the CBS domain of MgtE, it was decided to study the cytosolic domain separate from the rest of the protein. Due to uncertainty as to where the cytosolic domain ended and the transmembrane domain began, two DNA constructs were designed: MgtE CBS-L and MgtE CBS-S. Both encode the cytosolic domain of MgtE, which contains the N terminal, CBS domains and plug helix, but terminate at two different amino acids in the sequence of the connecting helix. As shown in Table 5, CBS-L is longer than CBS-S, possessing an extra 60 base-pairs.

Table 5– DNA constructs encoding the cytosolic domain of MgtE.

Designation	Molecular Weight (Da)	Amino Acid Sequence
MgtE CBS-L	32781.61	MVQNMTYDEL ILRIIILLRD GKIRDFRSVI DELQPYDMAF IFKEMPEKHR ARYLSYLTVD DITDMIGELE REFQLVVLNK VGKTKATLAM NKMDNDDLAQ LLEEMDEELK EQLLSSMEAS ESKAVQLLMN YPADSAGRMM TNRYVWIPQH YTVKDAVVKL KSFAEIAESI NYLYVINESK QLVGVLSYRD LILGEPEEKV QDLMFTRVIS ADALQDQEEV ARLIERYDFL AIPVVEENNV LVGIVTVDDI IDVVIREADE DYEKFAASGK DITFDTKAYV AAYR
MgtE CBS-S	30604.17	MVQNMTYDEL ILRIIILLRD GKIRDFRSVI DELQPYDMAF IFKEMPEKHR ARYLSYLTVD DITDMIGELE REFQLVVLNK VGKTKATLAM NKMDNDDLAQ LLEEMDEELK EQLLSSMEAS ESKAVQLLMN YPADSAGRMM TNRYVWIPQH YTVKDAVVKL KSFAEIAESI NYLYVINESK QLVGVLSYRD LILGEPEEKV QDLMFTRVIS ADALQDQEEV ARLIERYDFL AIPVVEENNV LVGIVTVDDI IDVVIREADE DYEK

2.3. Phenotype Complementation Assay

Complementation assays were performed by expression of full-length MgtE with and without expression of the DAC domain (with diadenylate cyclase activity) in the Mg^{2+}-uptake deficient *E. coli* strain TM2. MgtE was expressed from pBAD/HisB (Ampicillin-resistance), and DAC from pBAD33. pBAD33_DAC (Chloramphenicol-resistance) was obtained from previous experiments unrelated to this work (Marta Maria Noutel Lorga

Gomes, 2020). Empty vectors were used as negative controls. Protein expression from pBAD plasmids was induced with 0.02% L-arabinose.

In initial assays, transformed cells were plated onto LB20Mg agar plates containing the proper antibiotics (ampicillin at 100 µg/mL and chloramphenicol at 34 µg/mL) and grown overnight at 37 °C. Plates were then resuspended in 2 mL of LB and washed two times (by gentle centrifugation and resuspension in fresh LB) to ensure no excess Mg^{2+} from the plates was present. 5 mL of LB supplemented with varying concentrations of Mg^{2+} (0, 1, 2, 5, 10, 20, 50 mM) were inoculated with 2 µL of cells and grown overnight at 37 °C and 220rpm. The optical density of cultures was measured at 600nm to determine the Mg^{2+} concentration required for use in assays with minimal media.

The final conditions were the following: transformed cells were plated onto LB30Mg agar plates with antibiotics, grown overnight at 37 °C, resuspended in Minimal Media, and washed twice. 5 µL of cells were used to inoculate 5 mL of Minimal Media with varying concentrations of Mg^{2+} (0, 0.05, 0.1, 0.4, 30 mM) and induced with 0.02% arabinose. OD_{600nm} was measured after growing overnight at 37 °C, 220 rpm.

2.4. Protein Expression and Purification

The standard large-scale protocol for MgtE cytosolic domain expression and purification consists of the following steps: *E. coli* BL21(DE3) competent cells were transformed with pET24dT_CBS-L or pET24dT_CSB-S expression plasmids and plated onto LB plates containing 50 µg/mL kanamycin. The following day, plates were resuspended in LB media, and 4L culture flasks containing 1L LB media (with 50 µg/ml kanamycin) were inoculated with 2mL of resuspended cells. Cultures were grown in an orbital shaker at 37 °C, 160 rpm until OD_{600nm} reached 0.6~0.7, at which point cultures were immersed in an ice bath for 30 min for induction of cold-shock chaperones, followed by addition of 1% ethanol for induction of heat-shock chaperones and expression was induced by addition of 0.5 mM IPTG. Cultures were then incubated at 20 °C, 160 rpm overnight. Cells were pelleted by centrifugation (20 minutes, 3500 rpm, 4 °C) and stored at -20 °C.

Pellets were resuspended in 20 mL of Lysis Buffer (50 mM TrisHCl pH 8.0; 150 mM NaCl), followed by cell cracking using a pre-chilled Emulsifex-C5 (Avestin). Unwanted proteolytic digestion was inhibited by adding 1 mM PMSF, 1 µg/mL Leupeptin and 1µg/mL Pepstatin A prior to cell lysis. Lysate was centrifuged (45 minutes, 1700 rpm, 4 °C) and the supernatant was loaded into a pre-equilibrated cobalt affinity purification column. Beads were washed with 10 column volumes (CV) of Lysis buffer supplemented with 20mM Imidazole (MgtE CBS-L) or 10mM Imidazole (MgtE CBS-S). Bound protein was eluted using solutions with 20mM (10xCV), 50 mM (10xCV) and 150 mM (5xCV) of Imidazole; MgtE CBS-L was eluted with a minimum of 50 mM Imidazole. To assess which fractions contained protein, all eluted samples were analyzed by SDS-PAGE.

After addition of thrombin (2 µl), pooled fractions were dialyzed overnight against GF Buffer: 20mM TrisHCl pH8.0; 150 mM NaCl. The following day, dialyzed protein was concentrated and injected in a size-exclusion chromatography Superdex 200 10/300 GL

column (GE Healthcare), pre-equilibrated with GF Buffer. Eluted fractions were monitored by absorbance at 280 nm and elution peak fractions were submitted to SDS-PAGE analysis. Finally, purified protein fractions were pooled and concentrated. Protein concentration was determined by absorbance at 280nm using the extinction coefficient determined by ProtParam server (https://web.expasy.org/protparam/).

For isothermal titration calorimetry (ITC), GF Buffer was not adequate due to containing TrisHCl. Trisaminomethane (TRIS) possesses a high enthalpy of ionization that interferes with heat exchange measurements. As such, protein destined to ITC experiments was purified by size-exclusion using GFI Buffer (20 HEPES ph7.5;150 mM NaCl), as HEPES possesses a low enthalpy of ionization. (Goldberg, Kishore and Lennen, 2002)

2.5 Ligand Testing by Differential Scanning Fluorimetry (DSF)

Differential Scanning Fluorimetry (DSF) assays were carried out using a iQ5 real-time PCR detection system (Bio-Rad), with the Sypro Orange specific Cy3 optical filter (Ex: 490nm/Em: 575nm).

The initial assay involved MgtE CBS-L (in GF Buffer: 20 mM Tris pH8; 150 mM NaCl), and as a control, the KtrA protein in (in KtrA Buffer: 20 mM Tris pH 7.5; 150 mM KCl), a known ATP-activated regulatory protein of a K^+ transporter. KtrA was obtained from previous experiments unrelated to this work. Each sample contained either 5 µM or 10 µM of pure protein, 5x or 10x final concentration of SYPRO Orange Protein Gel Stain from two different stocks (A and B), and absence or presence of 1 mM of ATP. As a positive control, KtrA was not tested in the absence of ATP. The final sample volume was 50µL. Samples were assembled in a 96-well PCR White Plate (Bio-Rad) (Appendix, Scheme 1), then sealed and covered in aluminum foil. Temperature variation was set between 20 °C to 85 °C with a heating rate of 0.5 °C per 30 seconds.

Another assay was performed, involving both versions of the MgtE cytosolic domain (MgtE CBS-L and MgtE CBS-S) (in GF Buffer: 20 mM Tris pH8; 150 mM NaCl). For a final volume of 50 µL each sample contained: 10 µM of pure protein, 10x final concentration of SYPRO Orange Protein Gel Stain, absence or presence of 10 mM Mg^{2+}, and 0.5 mM of various ligands. Ligands used were c-di-AMP, ci-di-GMP, ppgpp, pppgpp, pApA, and DSMO (present as 2% v/v concentration). Mixtures were assembled in a 96-well PCR White Plate (Appendix, Scheme 2), sealed and covered in aluminum foil as previously done. Temperature variation was set between 20 °C to 85 °C with a heating rate of 0.5 °C per 30 seconds.

All data were analyzed using CFX Maestro (Bio-Rad) software.

2.6. X-Ray Crystallography

Crystallization screens were carried out using the sitting drop vapor diffusion method. Initially, two commercial screens were used, Morpheus and JCSG-plus (Molecular Dimensions), each with 96 different crystallization buffer conditions.

The purified MgtE CBS-S protein was concentrated to 8 mg/mL in GF+Mg Buffer (20mM Tris pH8; 150mM NaCl; 1mM Mg^{2+}), then centrifuged for 30 minutes at 13000g at 4°C in a table-top centrifuge to remove aggregates. To a portion of protein in buffer, c-di-AMP was added for a final concentration of 0.5mM, called GF+Mg+cdAMP buffer. The crystallization screen was carried out in 96-well 2-drop plates, sealed with transparent tape, and incubated at either 4°C or 20°C. Each well had two sitting drops, one prepared by adding protein in GF+Mg Buffer to reservoir solution (1:1 mix) and the other prepared by adding protein in GF+Mg+cdAMP Buffer to reservoir solution (1:1 mix). The final drop volume was 0.3µL, the reservoirs contained 40µL of crystallization solution, and the drops were set up using a robot (Oryx 4 by Douglas Instruments).

The initial screening was followed by optimizing of the best crystal-bearing conditions (solutions from Morpheus at 4°C), fine-tuning their components (buffer, precipitant and additives) in a 48-well plate (Appendix, Scheme 3) set by hand. Purified MgtE CBS-S was concentrated to 9.8 mg/mL in GF Buffer (20mM Tris pH8; 150mM NaCl), then centrifuged for 30 minutes at 13000g at 4 °C in a table-top centrifuge to remove aggregates. To the protein were added c-di-AMP (final concentration 0.5 mM) and varying amounts of Mg^{2+} (final concentrations 0 - 1mM). The reservoir volume was 150 µL and the drops had a final volume of 2µL, composed of a 1:1 mix of protein solution to reservoir solution. The plate was sealed and incubated at 4 °C.

Table 6– Composition of buffers used in the 48-well optimization plate.

Buffer System 2 pH 7.5	50.1% v/v MOPS (1 M); 49.9% v/v Sodium HEPES (1 M)
Precipitant Mix 2	60% v/v (40% v/v Ethylene glycol; 20 % w/v PEG 8000)
Carboxylic Acids Mix	0.2 M Sodium formate; 0.2 M Ammonium acetate; 0.2 M Sodium citrate tribasic dihydrate; 0.2M Potassium sodium tartrate tetrahydrate; 0.2 M Sodium oxamate
NPS Mix	0.3 M Sodium nitrate, 0.3 M Sodium phosphate dibasic, 0.3 M Ammonium sulfate

Since crystal growth conditions already contain cryoprotectants, crystals were collected from the drops and flash-frozen in liquid nitrogen immediately. They were then analyzed by X-ray diffraction at the synchrotron SOLEIL in Paris, France.

2.7. Isothermal Titration Calorimetry (ITC)

MgtE CBS-S protein was purified in GFI Buffer (20 mM HEPES pH7.5; 150 mM NaCl), after which it was dialyzed overnight against Dialysis Buffer (20 mM HEPES pH7.5; 150 mM NaCl) containing either 10 mM Mg^{2+} or no Mg^{2+}. Before the experiments, the protein was centrifuged for 30 minutes at 13000 g at 4 °C in a table-top centrifuge, in order to

remove any aggregates. Ligands used in each titration run were dissolved in Dialysis Buffer, with Mg^{2+} or without Mg^{2+}, matching the protein dialysis conditions.

In the initial titration runs, c-di-AMP (150 μM in the syringe) was titrated into MgtE CBS-S (10 μM in the sample cell) dialyzed either with magnesium or without magnesium. The volume of the first injection of the run was 2 μL, followed by 10 μL injections at 300s intervals.

In the follow-up titration runs, 200 μM of either c-di-AMP or ATP were titrated into 20 μM MgtE CBS-S samples dialyzed with magnesium. The volume of the first injection of the run was 2 μL, followed by 10 (ATP) or 15 (c-di-AMP) 3 μL injections, then by 5 μL, at 300s intervals.

The experiments were carried out using a MicroCal VP-ITC calorimeter (GE Healthcare) at 25 °C, with 300 μL of syringe volume and 1.4 mL of cell sample volume. All data was analyzed using Origin 7.0 (OriginLab) software, using a single binding site model.

2.8. Effect of c-di-AMP on the size-exclusion chromatography elution profile

To study if the cytosolic domain of MgtE undergoes a quaternary structure reorganization when it forms a complex with c-di-AMP, we used size-exclusion chromatography. Previously purified MgtE CBS-S samples at 145 μM, with and without 200 μM c-di-AMP, were injected in a Superdex 200 Increase 5/150 GL column (GE Healthcare), pre-equilibrated in a solution with GF Buffer (20 mM TrisHCl pH 8.0; 150 mM NaCl). The resulting chromatograms were then analyzed.

3. RESULTS AND DISCUSSION

3.1. Phenotype Complementation Assay

In order to investigate the function of the *B. subtilis* MgtE in the uptake of Mg^{2+}, we performed phenotype complementation assays using the *E. coli* triple mutant strain TM2, defective for the CorA, MgtE and YhiD Mg^{2+}-uptake systems, which requires over 10 mM Mg^{2+} in the media to grow. By transforming TM2 cells with a plasmid encoding *B. subtilis* MgtE, we could verify whether this protein acts as a Mg^{2+} channel. In addition, since *E. coli* lacks the enzymes responsible for c-di-AMP production, we could test the impact of c-di-AMP on MgtE function using TM2 co-transformed with plasmids encoding MgtE and the DAC domain (which synthesizes the dinucleotide).

MgtE was encoded in the pBADHisB_MgtE plasmid and the DAC domain in pBAD33_DAC. Empty plasmids were used as controls. pBADHisB and pBAD33 plasmids have compatible origins of replication and different antibiotic resistances (ampicillin and chloramphenicol, respectively). The two antibiotics were present throughout the different steps and phases of the work.

To confirm that MgtE promotes uptake of Mg^{2+}, TM2 cells were transformed with pBADHisB_MgtE and pBADHisB empty plasmid, induced with 0.02% L-arabinose, and grown in minimal media with no added Mg^{2+}, with 0.4 mM and30 mM Mg^{2+}.

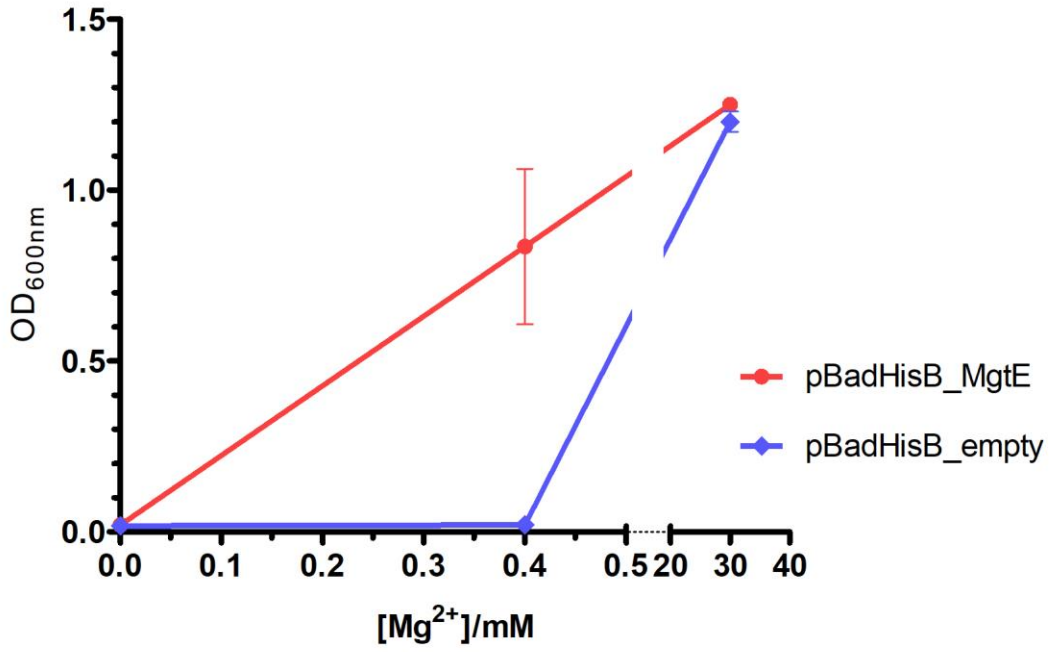

Figure 5– Growth curve of the *E. coli* TM2 mutant strain transformed with pBADHisB_MgtE or control plasmid pBADHisB.

Cell growth was performed on minimal medium supplemented with 0, 0.4 and 30 mM of Mg2+. Data represent averages of four independent experiments, with error bars representing the standard deviation.

As seen in Figure 5, MgtE rescues the TM2 mutant strain in 0.4 mM Mg^{2+}, confirming that MgtE is a Mg^{2+} channel.

To analyze the effect of c-di-AMP on the function of MgtE, TM2 cells were transformed with pBADHisB_MgtE and pBAD33_DAC or control plasmid pBAD33, induced with 0.02% L-arabinose, and grown in low concentrations of Mg^{2+} (0.05, 0.1, 0.4 mM), with a positive (30 mM) and negative control (0 mM). If c-di-AMP inactivates MgtE we would observe decreased overnight growth in the conditions where DAC is co-expressed. In contrast, if the nucleotide functions as an activator, then we would observe stronger growth when DAC is present.

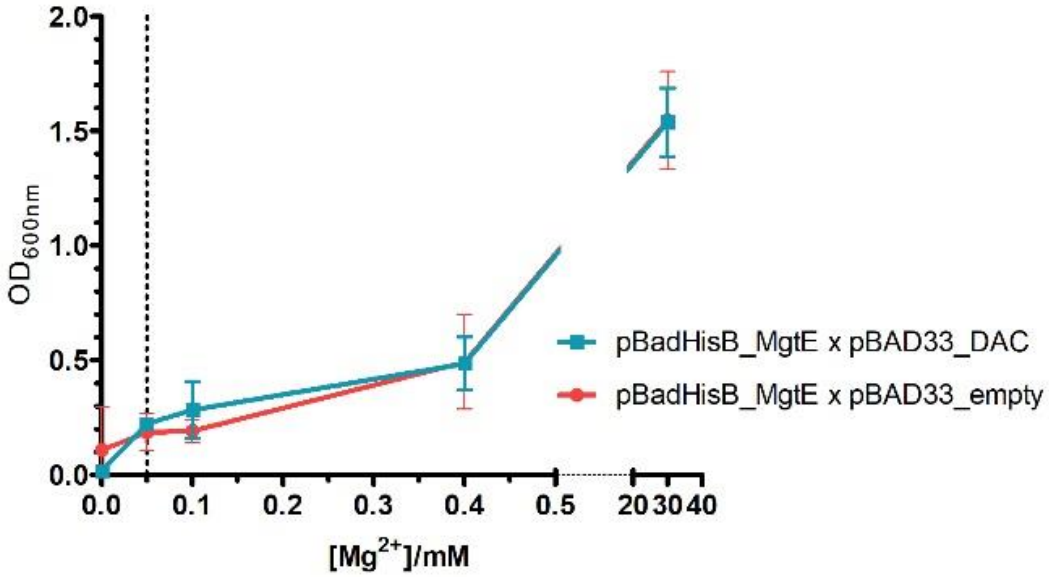

Figure 6– Growth curve of the *E. coli* TM2 mutant strain transformed with pBADHisB_MgtE and pBAD33_DAC or control plasmid pBAD33.

Cell growth was performed on minimal medium supplemented with 0, 0.05, 0.1, 0.4 and 30 mM of Mg^{2+}. The results represent the averages of five independent experiments, with error bars representing the standard deviations.

There are no visible differences in the growth curves obtained with and without DAC (Figure 6). The results obtained confirm that MgtE functions as a Mg^{2+} channel. However, the effect of c-di-AMP on its functionality were inconclusive, and thus further experiments need to be realized.

3.2. Protein Expression and Purification

3.2.1. Small-scale Protein Expression Test

To be able to characterize the biochemical and biophysical properties of the cytosolic domain of MgtE, we began by determining the best conditions for large-scale expression and purification of chosen constructs. Two different induction conditions (induction at 37

˚C for 3 hours or 20 ˚C overnight) were tested, and the levels of soluble protein expression were assessed.

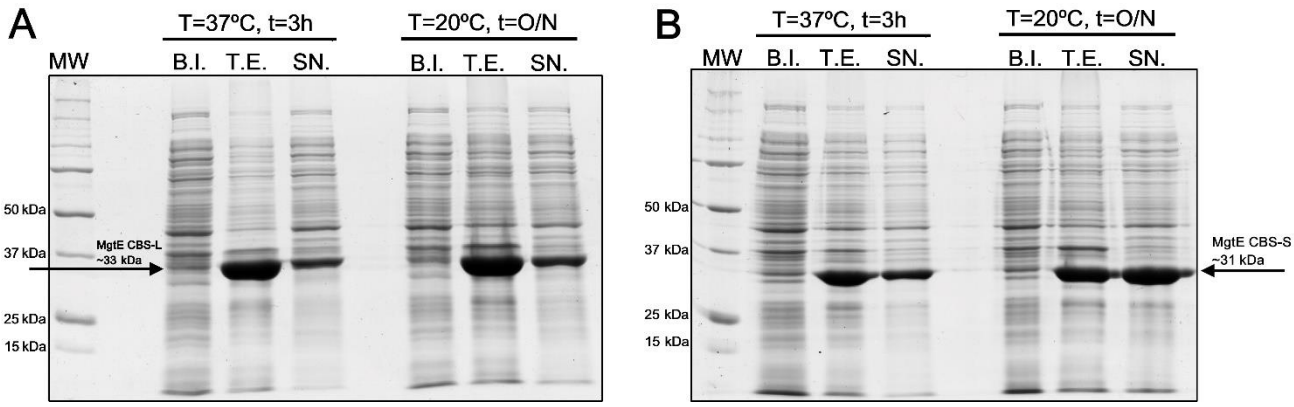

Figure 7– SDS-PAGE gels of MgtE's cytosolic domain induction test in BL21(DE3) *E. coli* strain.
(**A**) MgtE CBS-L induction test. (**B**) MgtE CBS-S induction test. Molecular weight protein markers (MW) are indicated on the left lane of each gel (Bio-Rad's Precision Plus Protein All Blue Prestained Protein Standards). Samples loaded on 12% SDS-PAGE gels are: total cell lysates before induction (B.I); cells lysed by sonication pre-centrifugation Total Extract (T.E.); and post-centrifugation supernatant (SN.). The expected position of the constructs is indicated by an arrow.

The gels analyzed (Figure 7) show that both MgtE CBS-L and MgtE CBS-S express in greater amounts after overnight induction at 20 °C. As such, overnight induction at 20 °C, as described in Section 2.4, was selected for all future protein preparations. Gels also show that at 20 ˚C there is a higher amount of MgtE CBS-S in the soluble fractions (present in the supernatant) than MgtE CBS-L. It suggests that MgtE CBS-S is more stable than MgtE CBS-L.

3.2.2. Purification of MgtE CBS-L

Purification of proteins typically involved a step of affinity chromatography in Co^{2+}-beads, which binds His-tagged proteins, cleavage of tag with a specific protease (thrombin) followed by size-exclusion chromatography. Fractions were collected during the purification steps and analyzed by SDS-PAGE to determine how the expressed protein was behaving in different conditions. Analysis of the protein's gel filtration chromatogram was also done to gather data on the oligomerization behavior of the protein.

Shown in Figure 8 is the SDS-PAGE of fractions collected from the affinity chromatography. It shows that large part of the protein was eluted in the first step of the washing process with 20 mM of Imidazole. This fraction also includes many other contaminant proteins greatly reducing the amount of pure protein collected after elution with high concentrations of imidazole. The digestion with thrombin is incomplete as seen by the presence of uncut protein band. The protein fractions eluted with 50 mM imidazole were pooled, concentrated and further purified by size-exclusion chromatography.

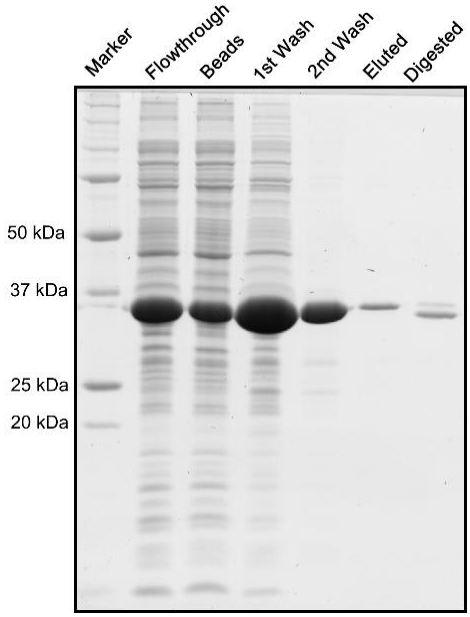

Figure 8– SDS-PAGE gel of the overall extraction and affinity column purification protocol for MgtE CBS-L.

A spin-cleared cell extract (Supernatant) was loaded in metal affinity purification column (Flowthrough); the beads were washed with 20 mM then 50mM Imidazole (1st Wash, 2nd Wash) and protein eluted with 150 mM Imidazole (Eluted). Overnight dialysis in the presence of thrombin yielded a fraction of tagless MgtE CBS-L (Digested). Marker: Bio-Rad's Precision Plus Protein All Blue Prestained Protein Standards.

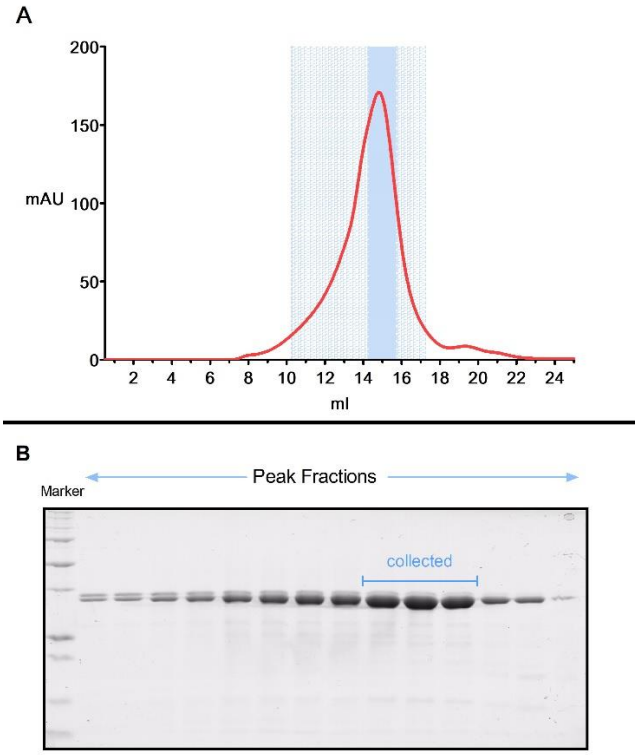

Figure 9– Size-exclusion chromatography results for MgtE CBS-L.

(**A**) Chromatogram of MgtE CBS-L purification. Peak fractions (0.5 mL) analyzed by SDS-PAGE from hatched blue area, final peak fractions collected from the blue area. **(B**) SDS-PAGE of peak fractions from size-exclusion chromatography. Marker used: Bio-Rad's Precision Plus Protein All Blue Prestained Protein Standards).

Through size exclusion chromatography, we were able to further clean the protein. As seen in Figure 9 A, MgtE CBS-L's chromatography profile includes a single peak, indicating a stable protein in the present conditions. Interestingly, the elution profile and SDS-PAGE of collected fractions show that protein elutes across a wide elution volume, from ~10 mL to 18 mL, suggesting the formation of several oligomeric protein forms that

are in equilibrium with each other. We decided to pool only fractions corresponding to the elution peak. The elution volume of this peak (~15 mL) is consistent with the formation of homodimers in the column used, by comparison with other proteins in the lab, as noted by Cereija et al in 2021 (found in Supplementary material).

The protocol developed and used for large-scale expression and purification of MgtE CBS-L yields approximately 56 µg of pure protein per liter of culture.

3.2.2. Purification of MgtE CBS-S

Large-scale purification of MgtE CBS-S was performed after MgtE CBS-L, with protocols adjusted to account for what had been previously discovered. The purification on a metal ion affinity column was modified to include an extra wash step with a lower concentration of Imidazole. It was expected that this would favor elution of contaminant proteins before elution of the cytosolic domain, increasing the amount of pure protein collected.

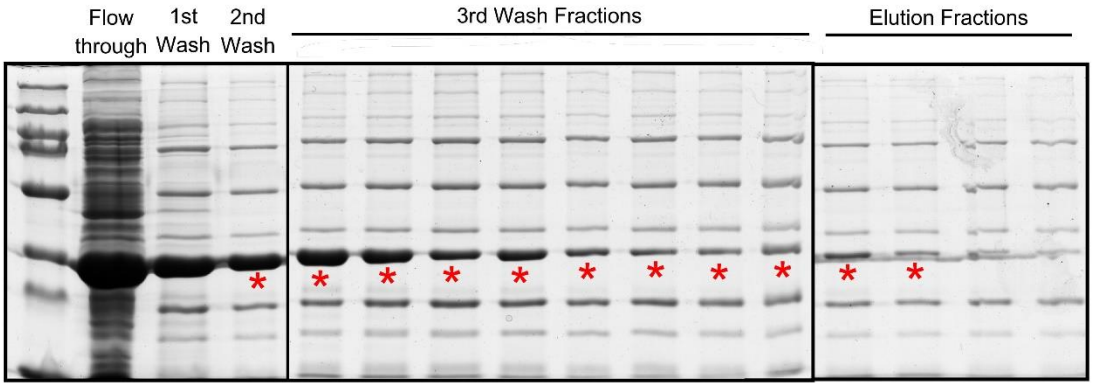

Figure 10– SDS-PAGE of fractions collected from affinity column purification of MgtE CBS-S.

Fractions selected for further purification are marked by asterisks (*). Spin-cleared cell extract was loaded in metal affinity purification column (Fow through); beads were washed with 10, 20 and 50 mM of Imidazole (1st Wash, 2nd Wash, 3r Wash) and protein eluted with 150 mM Imidazole (Elution). In this gel, the molecular weight standards are present in all lanes, mixed with the cytosolic protein, due to an error in sample preparation. Taking this in account it becomes clear that the cytosolic domain is already very pure in the 2nd wash fraction.

Figure 10 shows fractions collected from the cobalt affinity purification column. The addition of an extra wash step improved protein purity and increased its yield. We also note that there is a large amount of protein that did not bind to the cobalt beads, indicating that we needed to use a larger volume of beads for this step of purification.

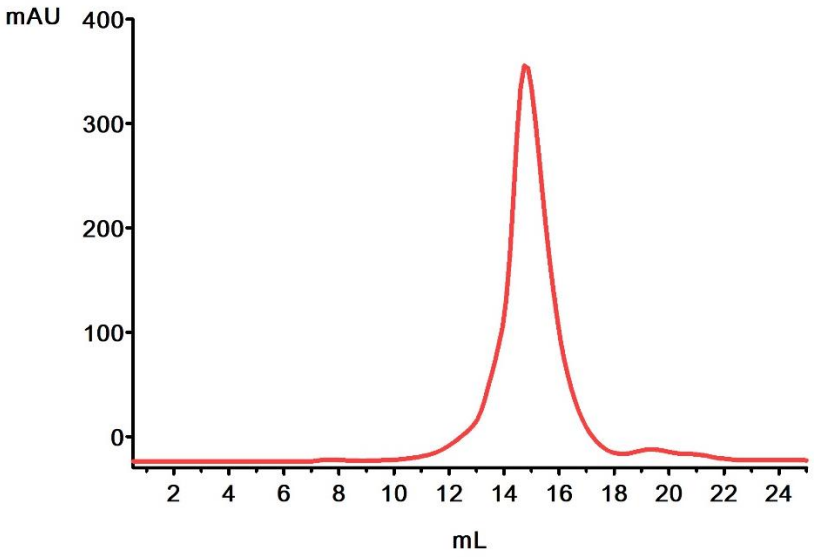

Figure 11– Size-exclusion chromatogram for MgtE CBS-S purification.

MgtE CBS-S produces a single sharp peak in size-exclusion chromatography, indicating that the protein is stable and monodisperse in the conditions used. Like MgtE CBS-L, the peak elutes at 14~15 mL. (Figure 11). Overall, MgtE CBS-S behaves better than MgtE CBS-L, producing a more regular chromatography profile.

The protocol developed and used for large-scale expression and purification of MgtE CBS-S yields approximately 3.25 mg of pure and well-behaved protein per liter of culture. This high protein yield makes it suitable for further biochemical and crystallography experiments.

3.3. Ligand Testing by Differential Scanning Fluorimetry (DSF)

It has been previously proposed that c-di-AMP binds to the CBS domain of MgtE. To confirm this proposal, an experiment was performed using the proteins MgtE CBS-L and MgtE CBS-S, encoding the cytosolic domain of MgtE, and differential scanning fluorimetry (DSF), also known as the Thermal Shift Assay. In this technique, a fluorescent dye (SYPRO Orange) that binds to the hydrophobic regions of proteins is used. The protein is incubated across a temperature gradient with SYPRO Orange; as temperature increases, the protein unfolds, exposing its hydrophobic regions and favoring SYPRO Orange binding, resulting in increased fluorescence. At higher temperatures, the protein aggregates, and fluorescence signal is reduced. Fluorescence intensity is plotted as a function of temperature and the mid-point transition temperature (T_m) between folded and unfolded states is calculated from the first derivative. Defined as the melting temperature, the T_m is a parameter typically associated with protein stability. Binding of a ligand to a protein will generally increase the T_m. When ΔT_m is greater than 2 °C, it is usually indicative that the molecule tested stabilizes the protein, making it a potential ligand. (Grøftehauge *et al.*, 2015)

We first attempted to determine the T_m and curve profile of MgtE CBS-L, using different concentrations of protein and fluorescent dyes. The ligand chosen was ATP, known to bind to the CBS domain of MgtE and increase the transporter's sensitivity to Mg^{2+} (Tomita *et al.*, 2017). The protein KtrA is known to bind ATP (Vieira-Pires, Szollosi and Morais-Cabral, 2013) and presents a well-defined thermal transition in this assay, therefore was chosen as a positive control. (Figure 12)

When compared with KtrA, the fluorescence profile of MgtE CBS-L as a function of temperature (or melting curve) showed a shallow transition due to high fluorescence at low temperatures. A starting high RFU value may indicate a tendency for cold unfolding, or that MgtE CBS-L possesses more exposed hydrophobic regions. From the first derivative plot, the melting temperature of MgtE CBS-L alone was defined as 46.8 ±0.8 °C (n=8). This value was compared with the melting temperature of the protein with ATP, but ΔT_m did not indicate that ATP stabilized the protein (Table 7). However, ATP appeared to improve slightly the profile of the melting curves (Figure 12). No significant difference was found between the different concentrations of MgtE CBS-L in the assay.

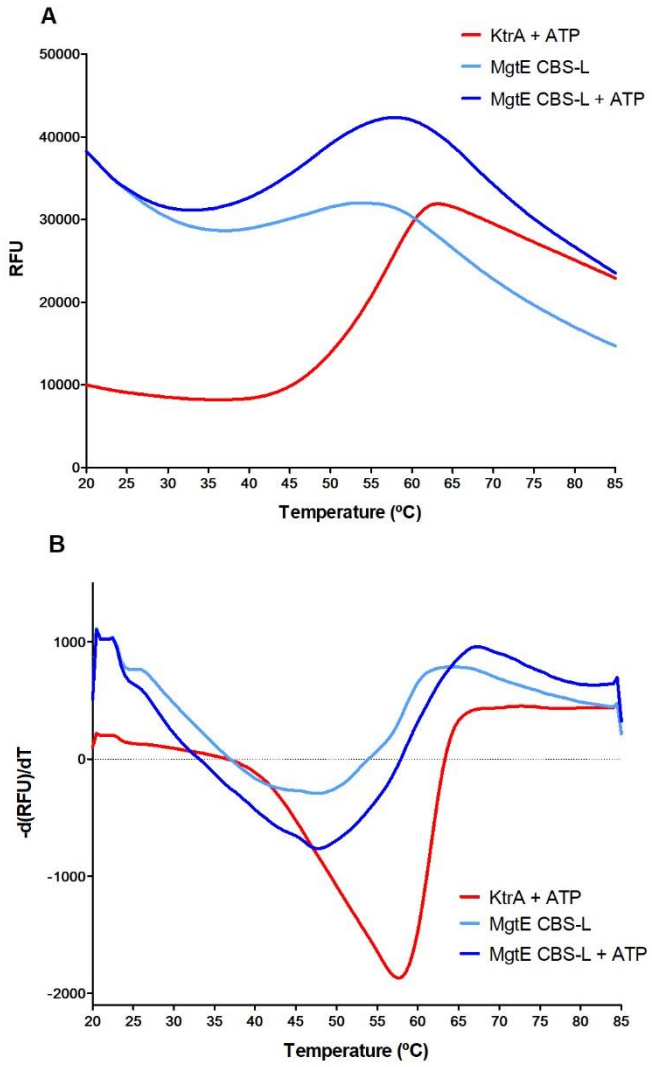

Figure 12– Differential Scanning Fluorimetry (DSF) profile for the CBS-L domain of MgtE, supplemented with ATP.

Representative (**A**) melting curves and (**B**) corresponding 1st derivative curves of MgtE CBS-L (10 μM) in the absence or presence of 1mM ATP. KtrA protein (10 μM) was used as a positive control.

Table 7– Melting temperature values [T_m (°C)] obtained for MgtE CBS-L and KtrA in the presence of ATP.

Legend: Number of replicas (n), standard deviation (SD) and thermal shift (ΔT_m).

	T_m (°C)	n	SD	ΔT_m (°C)
KtrA + ATP	57	16	0.7	--
MgtE CBS-L	46.8	16	0.8	--
MgtE CBS-L + ATP	47.1	16	0.8	+ 0.3

Having determined the T_m value for MgtE CBS-L, a follow-up assay was designed, intending to screen both MgtE CBS-L and MgtE CBS-S against several potential ligands,

including c-di-AMP and other nucleotide second messengers. The impact of Mg^{2+} was also studied. MgtE CBS-S, according to its behavior during protein purification, was hypothesized to be more stable.

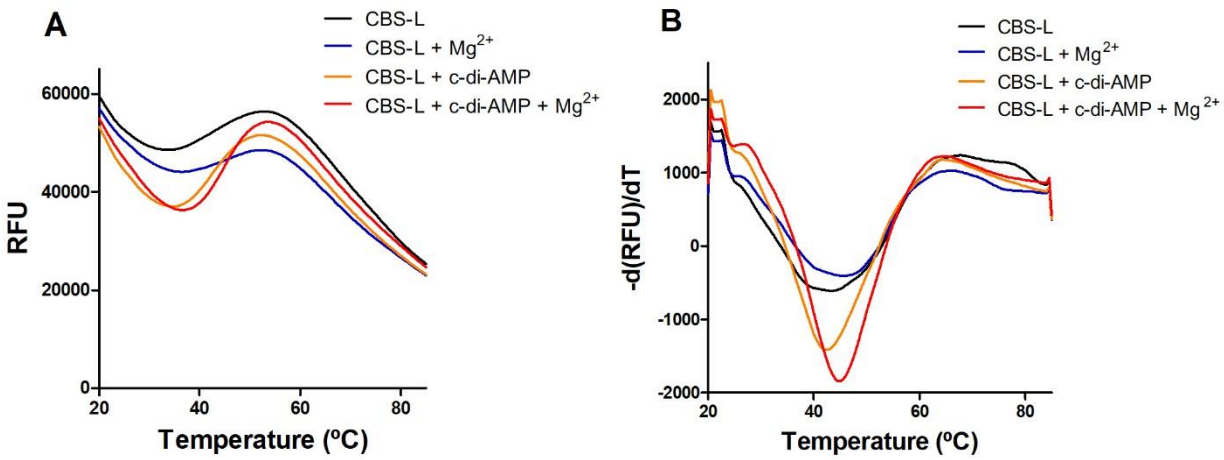

Figure 13– Differential Scanning Fluorimetry (DSF) assay results for the cytosolic domain of MgtE, supplemented with several potential ligands.

Representative (**A**) melting curves and (**B**) corresponding 1st derivative curves of MgtE CBS-L in the absence or presence of some of the potential ligands tested in the assay (Mg2+, c-di-AMP).

Table 8– Melting temperature values [T_m (°C)] obtained for MgtE CBS-L in the presence of Mg2+, c-di-AMP.

Thermal shift is determined relative to MgtE CBS-L alone. Legend: Number of repetitions (n), standard deviation (SD) and thermal shift (ΔT_m).

	T_m (°C)	n	SD	Δ T_m (°C)
MgtE CBS-L (follow-up assay)	42.3	3	2.4	-
MgtE CBS-L + Mg^{2+}	46.3	3	0.2	+ 4.0
MgtE CBS-L + c-di-AMP	42.3	3	0.2	0
MgtE CBS-L + c-di-AMP + Mg^{2+}	45	3	0.0	+ 2.7
MgtE CBS-L (initial assay)	46.8	16	0.8	-

As seen in Table 8, the T_m value determined for MgtE CBS-L during this second assay was inconsistent with the previously determined T_m. The high standard deviation associated with MgtE CBS-L measurements, combined with the low number of replicas, raises doubts about the results. Nevertheless, we determined ΔT_m for MgtE CBS-L in the presence of relevant ligands and the apo protein. The results indicate stabilization and binding of Mg^{2+} since there is a T_m shift of >2 °C. The presence of c-di-AMP does not alter the T_m but changes the melting curve profile (Figure 13), making it less shallow even in the presence of Mg^{2+}.

The experiments with MgtE CBS-S protein showed an increase in T_m relative to CBS-L domain (Table 10), supporting the increased stability of the shorter domain. Otherwise, the melting profiles of CBS-S with ligands showed similar changes to CBS-L. As seen in Figure 14, there is a clear change in profile of the melting curves measured in the presence of c-di-AMP. This effect is mainly due to a reduction in fluorescence signal at low temperatures and is specific to c-di-AMP, as c-di-GMP and other ligands do not show an appreciable effect. However, the T_m determined from the 1st derivative is reduced in the presence of c-di-AMP, which would suggest protein destabilization. We note that adding Mg^{2+} and c-di-AMP causes a clear increase in the T_m relative to having c-di-AMP alone, while keeping the improved profile of the melting curve. This effect is only observed with c-di-AMP.

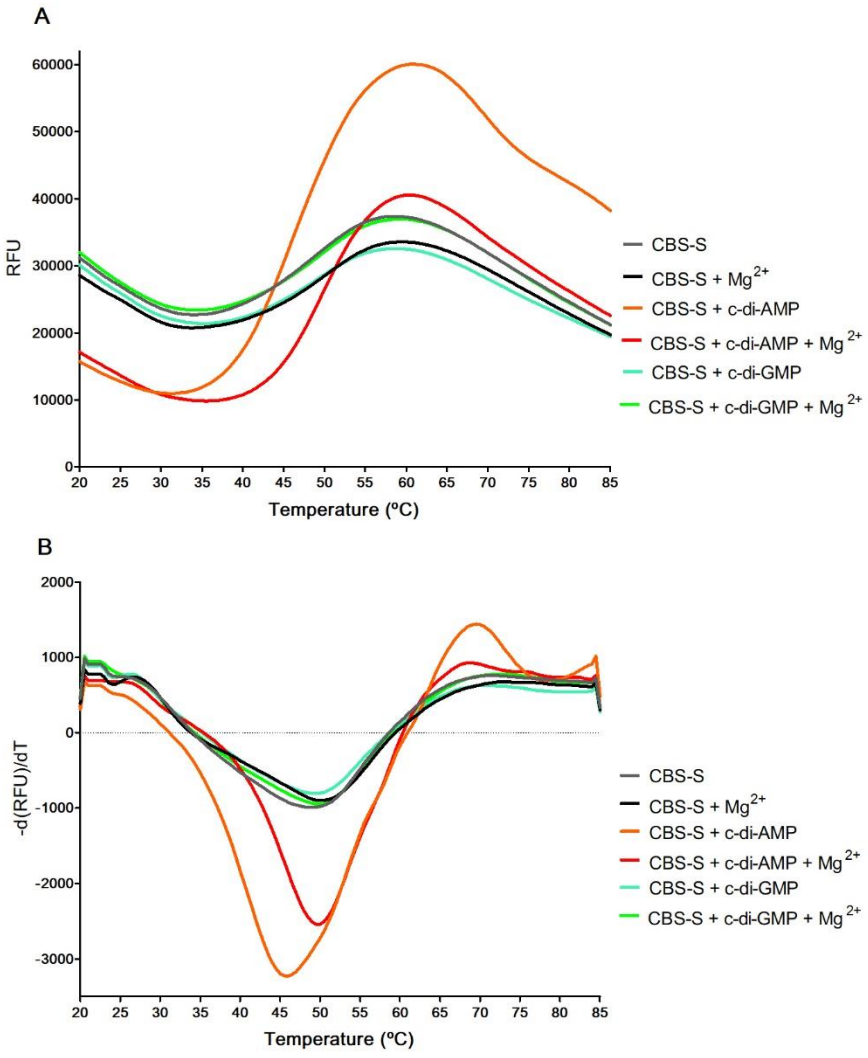

Figure 14– Differential Scanning Fluorimetry (DSF) assay results for the cytosolic domain of MgtE, supplemented with several potential ligands.

Representative (**A**) melting curves and (**B**) corresponding 1st derivative curves of MgtE CBS-S in the absence or presence of some of the potential ligands tested in the assay (Mg^{2+}, c-di-AMP, c-di-GMP).

Table 9– Melting temperature values [T_m (°C)] obtained for MgtE CBS-S in the presence of several ligands.

Legend: Standard deviation (SD) and thermal shift (ΔT_m).

Ligand	T_m (°C)	SD	Δ T_m (°C)
MgtE CBS-S control	49.5	0.4	-
+Mg^{2+}	50.0	0.0	+ 0.5
+c-di-AMP	45.8	1.4	- 3.5
+c-di-AMP + Mg^{2+}	49.8	0.2	+ 0.3
+c-di-GMP	49.5	0.0	0
+c-di-GMP + Mg^{2+}	50.0	0.0	+ 0.5
+pApA	49.5	0.0	0
+pApA + Mg^{2+}	50.0	0.4	+ 0.5
+pppgpp	49.3	0.6	- 0.2
+pppgpp + Mg^{2+}	50.2	0.2	+ 0.7
+ppgpp	50.0	0.0	+ 0.5
+ppgpp + Mg^{2+}	50.0	0.4	+ 0.5
+DMSO	50.0	0.0	+ 0.5
+DMSO + Mg^{2+}	50.0	0.0	+ 0.5

Table 10– Comparison between melting temperature values [T_m (°C)] obtained for MgtE CBS-S and MgtE CBS-L.

Legend: Standard deviation (SD) and thermal shift (ΔT_m).

	MgtE CBS-L			MgtE CBS-S		
Ligand	T_m (°C)	SD	Δ T_m (°C)	T_m (°C)	SD	Δ T_m (°C)
No ligand	42.5	2.4	-	49.5	0.4	-
+Mg^{2+}	46.3	0.2	+ 4.0	50.0	0.0	+ 0.5
+c-di-AMP	42.3	0.2	0	45.8	1.4	- 3.5
+c-di-AMP + Mg^{2+}	45.0	0.0	+ 2.7	49.8	0.2	+ 0.3

The apparently stabilizing influence of Mg^{2+} on the possible MgtE and c-di-AMP complex, and the thermal shift observed with MgtE CBS-L, confirm that Mg^{2+} is a ligand of the cytosolic domain of MgtE from *B. subtilis*. This is consistent with previously published

data regarding MgtE (Hattori *et al.*, 2007, 2009). Interestingly, these results also suggest a link between c-di-AMP and Mg^{2+} binding. They also suggest that c-di-AMP is a ligand, due to its effects on the fluorescence profile and melting temperatures, while suggesting that ATP might not be a ligand.

Due to its behavior during this experiment, appearing to be more stable (lower starting RFU values) and generating more consistent results, MgtE CBS-S was chosen as the protein construct to use in all further experiments.

3.4. Isothermal Titration Calorimetry (ITC)

To better characterize the binding of c-di-AMP to MgtE, isothermal titration calorimetry (ITC) was used. ITC is a technique where upon titration of ligand, heat changes (positive or negative) are measured by the instrument as a molecular complex is formed. As the ligand saturates the protein's binding sites, the heat changes measured per injection decrease to zero. Analysis of the titration curve allows for the determination of binding enthalpy (ΔH), the association constant (K_A) and the stoichiometry of the binding reaction (n). (Leavitt and Freire, 2001; Srivastava and Yadav, 2019)

Experiments were performed to characterize the cytosolic domain of MgtE and c-di-AMP binding reaction, in the presence and absence of Mg^{2+}, and the MgtE cytosolic domain of MgtE and ATP binding reaction. Once again, we chose to use the construct MgtE CBS-S for its stability and for the results shown during the thermal shift assay. The protein was purified and titrated as described in Section 2.7.

Single titration experiments of MgtE CBS with c-di-AMP in the presence or absence of Mg^{2+} show an exothermic binding reaction with c-di-AMP binding to MgtE CBS-S in both conditions (Figure 15 A and B and Table 11). We did not observe differences between the two conditions, either in the binding enthalpy of the reaction, -47.72 kcal/mol with Mg^{2+} and -45.35 kcal/mol without Mg^{2+}, or in the dissociating constant K_D (calculated from K_A), 1.75 μM without Mg^{2+} and 1.13 μM with Mg^{2+}. The measured K_D values are within the range of expected c-di-AMP concentrations in *B. subtilis*, low micromolar (Oppenheimer-Shaanan *et al.*, 2011). Surprisingly, the stoichiometry (n) of the interaction is approximately 0.25, whether Mg^{2+} is present or not. This either indicates that a large fraction of the cytosolic domain is incompetent to bind ligand (for example, it is unfolded), or that we have greatly over-estimated the protein concentration, or that a single c-di-AMP molecule binds to 4 MgtE CBS-S molecules. This is an interesting result, because MgtE is known to form dimers, not tetramers, and as such we would be expecting n=0.5.

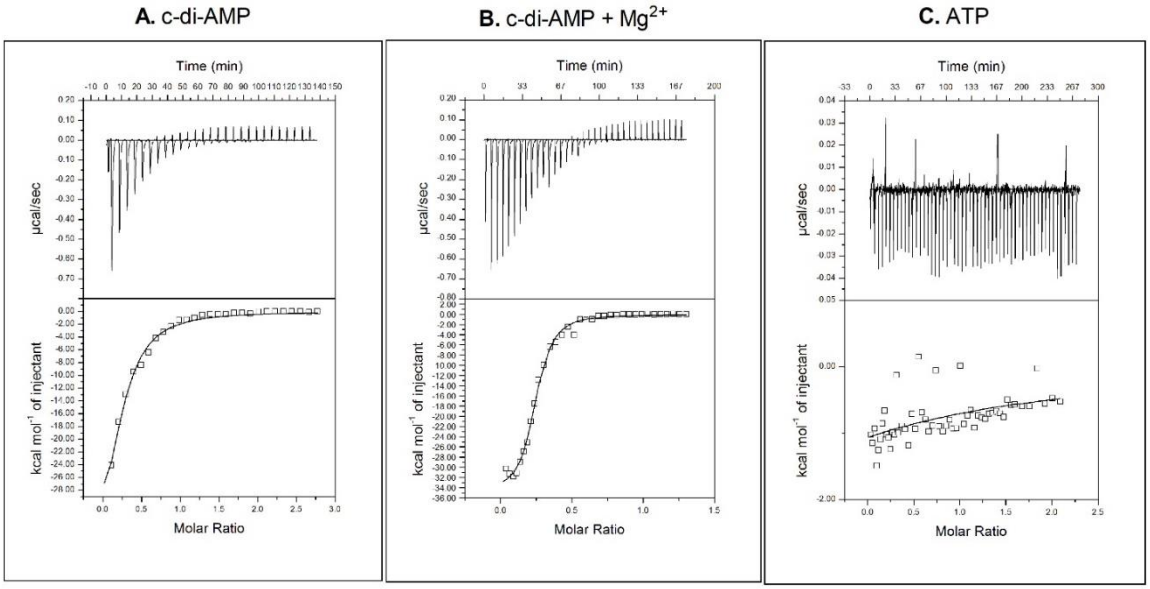

Figure 15 - ITC data of the MgtE cytosolic domain with (A) c-di-AMP (B) c-di-AMP and Mg^{2+} (C) ATP.

The raw ITC data (top panel) and profiles (bottom panel) are shown.

Table 11– Values of binding enthalpy (ΔH), association constant (K_A) and stoichiometry (n) obtained by data fitting.

	c-di-AMP	c-di-AMP + Mg^{2+}	ATP
ΔH	$4.535x10^4$ ±5479 cal/mol	$-4.772x10^4$ ±467.1 cal/mol	$-8.393x10^4$ ±$2.889x10^7$ cal/mol
K_A	$5.73x10^5$±$8.07x10^4$ M^{-1}	$8.83x10^6$ ±$5.30x10^5$ M^{-1}	$6.67x10^3$ ±$6.92x10^4$ M^{-1}
n	0.240 ±0242	0.267 ±0.00179	0.0965 ±32.7

In contrast, the titration of MgtE CBS-S with ATP, in the presence of Mg^{2+}, shows a very shallow curve (Figure 15 C) that likely indicates no interaction or a very weak interaction between the protein and ATP. Analysis of the data gave rise to a dissociating constant K_D ~150 µM (Table 11), which is roughly consistent with previously published results that set the K_D of MgtE for ATP in the presence of Mg^{2+} at 172 µM. (Tomita *et al.*, 2017)

Overall, these results are consistent with the results shown in the Differential Scanning Fluorimetry assay. They confirm the binding of c-di-AMP to the cytosolic domain of MgtE. They also indicate possible preference for c-di-AMP over ATP, the latter displaying a lower affinity for MgtE CBS-S.

3.5. Size-exclusion Chromatography

The stoichiometry of c-di-AMP binding determined by ITC suggests that the cytosolic domain upon ligand binding should be a tetramer. Since our size-exclusion chromatography experiments (Figure 11) indicate that the domain is a dimer in the absence of dinucleotide, we wondered if oligomerization can be detected by size-exclusion chromatography. To study the effect of binding between c-di-AMP and the cytosolic domain of MgtE, we compared the elution profile of MgtE CBS-S alone with that of MgtE incubated with 200 µM c-di-AMP. For this analysis we used a Superdex 200 Increase 5/150 GL column, with a total volume of 3 mL, which will result in a lower dilution of the protein during the chromatography run and a higher probability of detecting weakly interacting complexes.

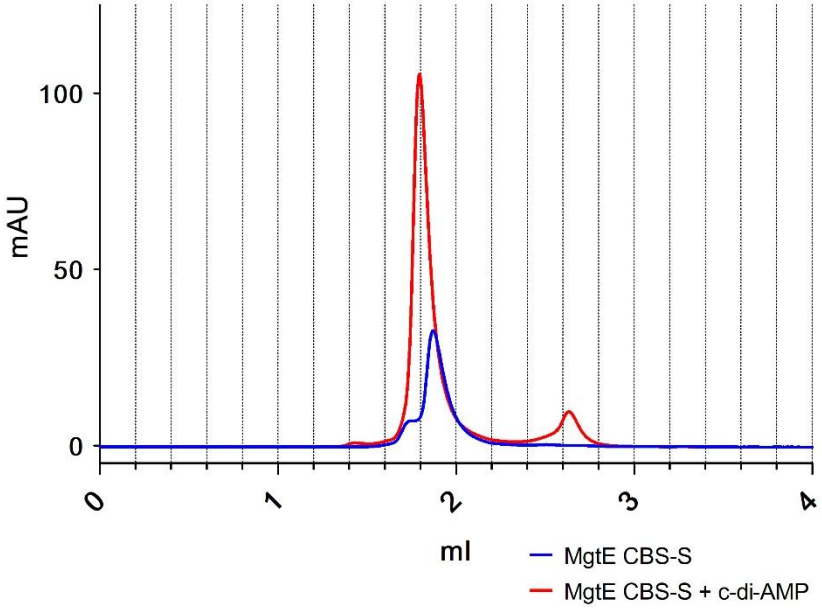

Figure 16 - Effect of c-di-AMP on the cytosolic domain of MgtE, monitored by size exclusion chromatography.

As shown above in red (Figure 16), in the presence of c-di-AMP, the protein presents a very sharp elution peak at 1.8 mL. At ~2.6 mL, a smaller peak indicates the elution of a smaller molecule, likely some fraction of excess c-di-AMP that did not bind to the protein. In contrast, the chromatogram of MgtE CBS-S without c-di-AMP (in blue) shows a peak with smaller height that is slightly shifted to higher elution volumes (~1.9 ml). Since we loaded the same amount of protein in both runs, the increase in peak height is consistent with association of the nucleotide, which absorbs strongly at 260 nm, with the protein. The shift in elution volume is consistent with a change in oligomerization or conformation when c-di-AMP binds to MgtE CBS-S.

A change in oligomerization is consistent with the results from ITC and confirms that c-di-AMP binds to the cytosolic domain of MgtE.

3.6. Crystallography Studies

In 2007, Hattori et al. published the structure of MgtE from *Thermus thermophilus*, as well as the structure of its cytosolic domain, spanning the N-terminal and CBS domains, in the presence and absence of Mg^{2+}. There is no experiment information available about the structure of MgtE bound to c-di-AMP, nor of MgtE from *B. subtilis*. Obtaining a three-dimensional structure of the protein bound to this ligand is decisive to understanding the molecular and biochemical properties of both molecules together. For this purpose, we chose to attempt crystallization using the construct MgtE CBS-S, shown to be more stable in previous assays, and having a higher melting point (T_m), which could indicate a greater stability at lower temperatures and a greater chance of successful crystal formation (Grøftehauge *et al.*, 2015).

Initially, a random screening with two commercially available crystallization screens was performed, Morpheus and JCSG-plus, at 4 °C and 20 °C. As described in Section 2.6, MgtE CBS-S was tested using the sitting drop vapor diffusion method, supplemented with Mg^{2+} alone, or c-di-AMP and Mg^{2+}.This approach was successful (Figure 17) and the formation of crystals was confirmed in several conditions, listed in Table 12. Notably, no crystals were formed at 20°C or without the presence of c-di-AMP.

Table 12– Crystallization hits obtained for MgtE CBS-S bound to c-di-AMP and Mg2+ using commercial screening conditions (Morpheus and JCSG-plus, from Molecular Dimensions).

Crystallization Condition	Screen	Temperature
B10 (0.09M Halogens; 0.1M Buffer System 3 pH8.5; 30% v/v Precipitant Mix 2)	Morpheus	4°C
C6 (0.09M NPS; 0.1M Buffer System 2 pH7.5; 30% v/v Precipitant Mix 2)	Morpheus	4°C
C10 (0.09M NPS; 0.1M Buffer System 3 pH8.5 30% v/v Precipitant Mix 2)	Morpheus	4°C
D10 (0.12M Alcohols; 0.1M Buffer System 3 pH8.5; 30% v/v Precipitant Mix 2)	Morpheus	4°C
F10 (0.12M Monosaccharides; 0.1 M Buffer System 3 pH8.5; 30% v/v Precipitant Mix 2)	Morpheus	4°C
G6 (0.1M Carboxylic acids; 0.1M Buffer System 2 pH7.5; 30% v/v Precipitant Mix 2)	Morpheus	4°C
G7 (0.1M Carboxylic acids; 0.1M Buffer System 2 pH7.5; 30% v/v Precipitant Mix 3)	Morpheus	4°C
G10 (0.1M Carboxylic acids; 0.1M Buffer System 3 pH8.5; 30% v/v Precipitant Mix 2)	Morpheus	4°C
H10 (0.1M Amino acids; 0.1M Buffer System 3 pH8.5; 30% v/v Precipitant Mix 2)	Morpheus	4°C

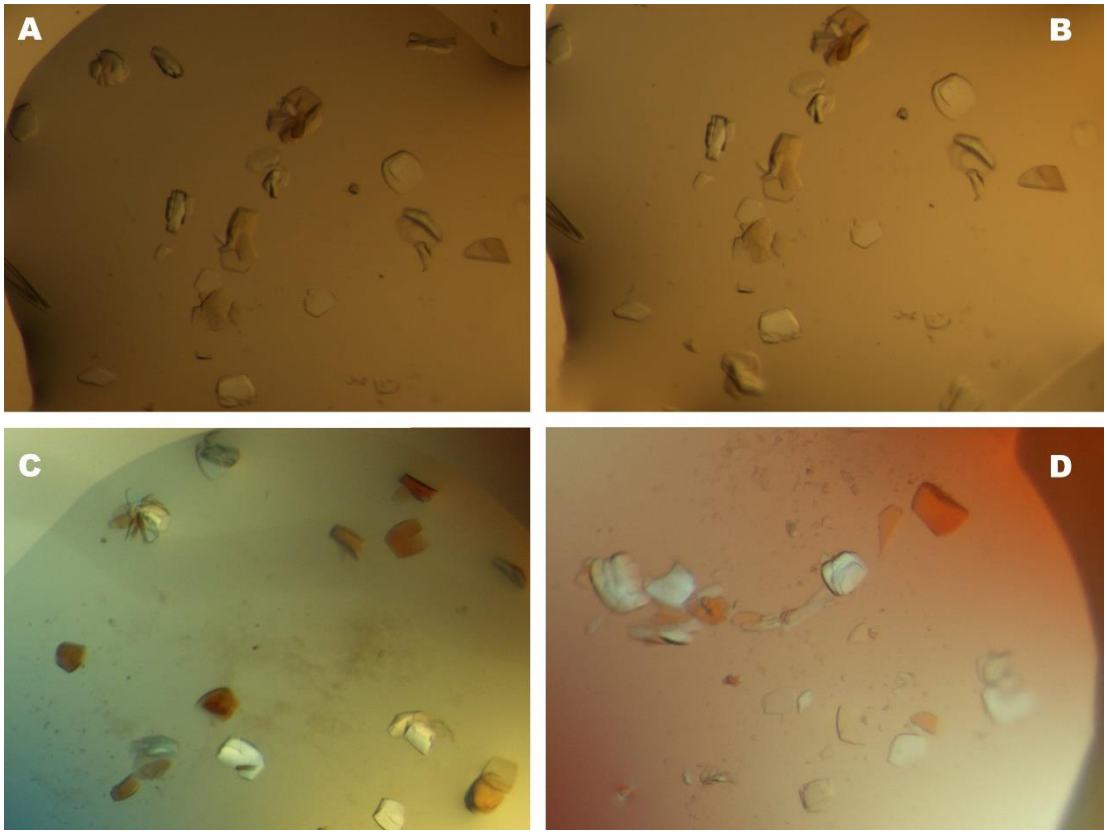

Figure 17– Examples of crystals obtained from initial screening assay.
Screen used was Morpheus from Molecular Dimensions, at 4°C. (**A**) Condition B10: 0.09M Halogens; 0.1M Buffer System 3 pH8.5; 30% v/v Precipitant Mix 2. (**B**) Condition C10: 0.09M NPS; 0.1M Buffer System 3 pH8.5 30% v/v Precipitant Mix 2. (**C**) Condition G10: 0.1M Carboxylic acids; 0.1M Buffer System 3 pH8.5; 30% v/v Precipitant Mix 2. (**D**) Condition C6: 0.09M NPS; 0.1M Buffer System 2 pH7.5; 30% v/v Precipitant Mix 2.

A homemade screen was developed to reproduce and optimize crystal size and nucleation. Conditions C6 and G6 of Morpheus, having produced good crystals, were explored further by varying the percentage of precipitant mix and Mg^{2+} concentration (as shown in Table 6), and incubated at 4°C. The assay successfully produced crystals in several conditions (Figure 18 and Table 13).

Table 13– Crystallization hits obtained for MgtE CBS-S bound to c-di-AMP during follow-up optimization assay.

Crystallization Condition
B3: 0.1M Buffer System 2 pH7.5, 0.1M Carboxylic Acids Mix, 24% v/v Precipitant Mix 2, 1mM Mg^{2+}
D1: 0.1M Buffer System 2 pH7.5, 0.1M Carboxylic Acids Mix, 28% v/v Precipitant Mix 2, 0mM Mg^{2+}
E1: 0.1M Buffer System 2 pH7.5, 0.1M Carboxylic Acids Mix, 30% v/v Precipitant Mix 2, 0mM Mg^{2+}
G1: 0.1M Buffer System 2 pH7.5, 0.1M Carboxylic Acids Mix, 34% v/v Precipitant Mix 2, 0mM Mg^{2+}
G2: 0.1M Buffer System 2 pH7.5, 0.1M Carboxylic Acids Mix, 34% v/v Precipitant Mix 2, 0.5mM Mg^{2+}
G4: 0.1M Buffer System 2 pH7.5, 0.9M NPS Mix, 34% v/v Precipitant Mix 2, 0mM Mg^{2+}
G5: 0.1M Buffer System 2 pH7.5, 0.9M NPS Mix, 34% v/v Precipitant Mix 2, 0.5mM Mg^{2+}
H1: 0.1M Buffer System 2 pH7.5, 0.1M Carboxylic Acids Mix, 36% v/v Precipitant Mix 2, 0mM Mg^{2+}
H2: 0.1M Buffer System 2 pH7.5, 0.1M Carboxylic Acids Mix, 36% v/v Precipitant Mix 2, 0.5mM Mg^{2+}

H3: 0.1M Buffer System 2 pH7.5, 0.1M Carboxylic Acids Mix, 36% v/v Precipitant Mix 2, 1mM Mg^{2+}
H4: 0.1M Buffer System 2 pH7.5, 0.9M NPS Mix, 36% v/v Precipitant Mix 2, 0mM Mg^{2+}
H5: 0.1M Buffer System 2 pH7.5, 0.9M NPS Mix, 36% v/v Precipitant Mix 2, 0.5mM Mg^{2+}
H6: 0.1M Buffer System 2 pH7.5, 0.9M NPS Mix, 36% v/v Precipitant Mix 2, 1mM Mg^{2+}

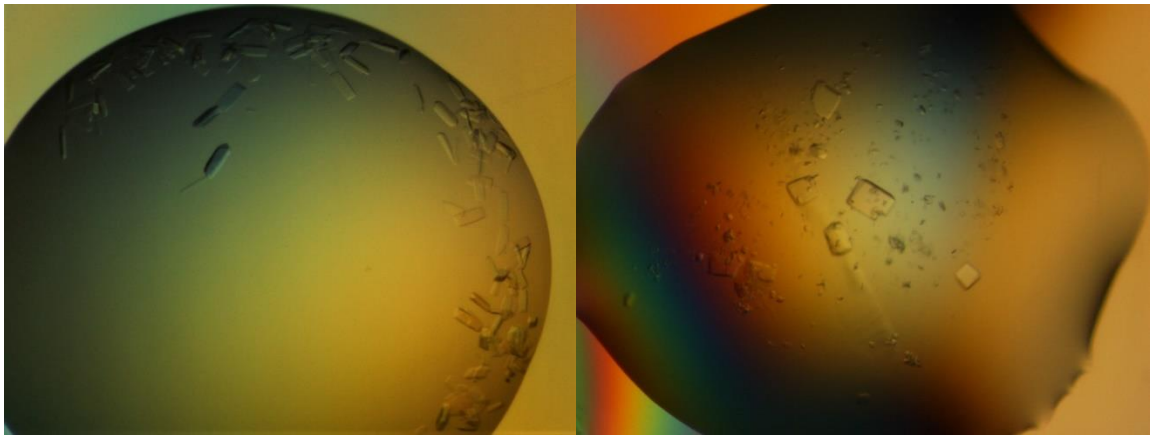

Figure 18– Examples of crystals obtained from optimization assay.
Left: crystals obtained in optimization screen condition G1 (0.1M Buffer System 2 pH7.5, 0.1M Carboxylic Acids Mix, 34% v/v Precipitant Mix 2, 0mM Mg2+). Right: crystals obtained in optimization screen condition H1 (0.1M Buffer System 2 pH7.5, 0.1M Carboxylic Acids Mix, 36% v/v Precipitant Mix 2, 0mM Mg2+).

Crystals from both assays were harvested and analyzed by X-ray diffraction. Some data sets were collected, but the diffraction patterns showed low quality, with elongated spots indicative of broken or multiple crystals, that did not allow the resolution of the structure of MgtE cytosolic domain when bound to c-di-AMP. Most crystals diffracted to 8Å, with the best patterns going up to 4-5Å. The great majority of crystals presented anisotropy, clearly visible in their diffraction patterns, longer in one direction than the other (Figure 19).

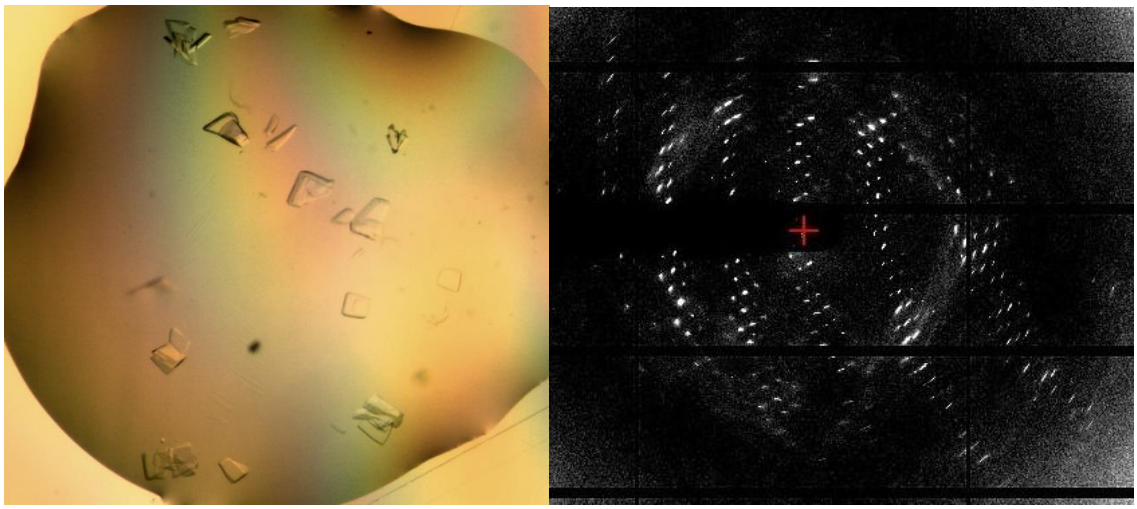

Figure 19– Examples of crystals obtained from handmade optimization assay and corresponding diffraction pattern collected using synchrotron radiation from an exemplar.
Left, crystals obtained in optimization screen condition H4 (0.1M Buffer System 2 pH7.5, 0.9M NPS Mix, 36% v/v Precipitant Mix 2, 0mM Mg2+). Right, the diffraction pattern from one of the crystals depicted;

diffraction pattern characterization was not achieved due to the low quality of the diffraction spots (smeared shape); the anisotropic nature of the crystal is evident from the diffraction pattern.

4. CONCLUSIONS

The main objectives for this work were: to confirm that the second messenger molecule c-di-AMP binds to the CBS domain of MgtE as previously proposed (Gundlach *et al.*, 2019); and to determine if c-di-AMP had a role in MgtE-mediated Mg^{2+} transport.

In summary, to study the CBS domain of MgtE, we designed DNA constructs that encoded the cytosolic domain of MgtE and established a protocol for large-scale expression and purification of both protein constructs. Appropriate amounts of high-quality pure protein were obtained, validating our protocols, and allowing for experiments meant to identify and characterize the connection between our objects of study.

Potential ligands were screened by differential scanning fluorometry, and results indicate that c-di-AMP is likely to be a ligand of the cytosolic domain. Furthermore, Mg^{2+} was found to increase the T_m of the domain only in the presence of c-di-AMP, suggesting an interplay in the binding of the two ligands. However, ITC characterization of the binding reaction between the cytosolic domain of MgtE and c-di-AMP showed no alterations when Mg^{2+} is present or absent. C-di-AMP binds to the cytosolic domain with a K_D of 1.75 μM in the absence of Mg^{2+}, within the range of expected c-di-AMP concentrations in *B. subtilis.* In the presence of Mg^{2+} the K_D was 1.13 μM. Stoichiometry, interestingly, was shown to be 1 c-di-AMP molecule per 4 MgtE molecules, which did not match expected oligomerization. Size-exclusion chromatography experiments were designed to clarify the situation. They revealed that the cytosolic domain of MgtE went through a conformational change when in the presence of c-di-AMP, once again confirming that c-di-AMP bound to the cytosolic domain of the channel, that is consistent with a reorganization of the quaternary structure.

Crystallization of the isolated cytosolic domain of MgtE was attempted, performed in the presence and absence of c-di-AMP. Several crystals could be grown in the presence of c-di-AMP but not in its absence, further cementing c-di-AMP's stabilizing influence. However, the quality of the diffraction data collected was unsatisfactory and the protein structure could not be resolved.

Complementation studies in *E. coli* mutant strains were performed to decipher c-di-AMP functional impact on MgtE activity. Unfortunately, results were inconclusive, and we could not determine if c-di-AMP affects MgtE. The growth curves obtained did not present significant differences. In parallel, differential scanning fluorimetry did not provide any indication that ATP bind to MgtE's cytosolic domain. ITC is suggestive that if ATP binds, it is with low affinity. ATP has been proven to bind to wild type MgtE from *T. thermophilus*, with a measured K_D equal to ours (Tomita *et al.*, 2017). It must be noted that the intracellular concentration of ATP is in the millimolar range while c-di-AMP is in the micromolar range (Oppenheimer-Shaanan *et al.*, 2011), so while MgtE might prefer c-di-AMP, ATP is far more readily available. The K_D values we have measured for each ligand are therefore suggestive of a functional effect for both. In the end, one of the main goals of this work was achieved: in *B. subtilis*, cyclic di-AMP binds to the channel MgtE at its cytosolic domain. However, the functional role of c-di-AMP remains uncharacterized.

Further experiments and functional assays are necessary to determine how, or if, the binding of c-di-AMP and MgtE affects Mg^{2+} transport in some way. Crystallographic studies to determine the structure of the cytosolic domain of MgtE in complex with c-di-AMP will elucidate the structural changes that are suggested by our results. We remark also that Mg^{2+} was consistently found to interplay with c-di-AMP binding in the structural stabilization of the cytosolic domain of MgtE. Further studies of that interaction by ITC will be necessary to completely understand the mechanisms of modulation involved. A titration of Mg^{2+} into a mixture containing protein saturated with c-di-AMP or ATP, will reveal the impact of nucleotide binding on the interaction with the well characterized modulator of MgtE function. Finally, it will be important to express, purify and analyze the function of full-length MgtE (through electrophysiology or a liposome-based flux assay) and its dependence of Mg^{2+}, c-di-AMP and ATP.

REFERENCES

de Baaij, J.H.F., Hoenderop, J.G.J. and Bindels, R.J.M. (2015) 'Magnesium in Man: Implications for Health and Disease', *Physiological Reviews*, 95(1), pp. 1–46. Available at: https://doi.org/10.1152/physrev.00012.2014.

Began, J. *et al.* (2020) 'Rhomboid intramembrane protease YqgP licenses bacterial membrane protein quality control as adaptor of FtsH AAA protease', *The EMBO Journal*, 39(10). Available at: https://doi.org/10.15252/embj.2019102935.

Burdette, D.L. *et al.* (2011) 'STING is a direct innate immune sensor of cyclic di-GMP', *Nature*, 478(7370), pp. 515–518. Available at: https://doi.org/10.1038/nature10429.

Cereija, T.B. *et al.* (2021) 'c-di-AMP, a likely master regulator of bacterial K^+ homeostasis machinery, activates a K^+ exporter', *Proceedings of the National Academy of Sciences*, 118(14), p. e2020653118. Available at: https://doi.org/10.1073/pnas.2020653118.

Corrigan, R.M. *et al.* (2011) 'c-di-AMP Is a New Second Messenger in Staphylococcus aureus with a Role in Controlling Cell Size and Envelope Stress', *PLoS Pathogens*. Edited by A. Cheung, 7(9), p. e1002217. Available at: https://doi.org/10.1371/journal.ppat.1002217.

Corrigan, R.M. and Gründling, A. (2013) 'Cyclic di-AMP: another second messenger enters the fray', *Nature Reviews Microbiology*, 11(8), pp. 513–524. Available at: https://doi.org/10.1038/nrmicro3069.

DiNicolantonio, J.J., O'Keefe, J.H. and Wilson, W. (2018) 'Subclinical magnesium deficiency: a principal driver of cardiovascular disease and a public health crisis', *Open Heart*, 5(1), p. e000668. Available at: https://doi.org/10.1136/openhrt-2017-000668.

Franken, G.A.C. *et al.* (2022) 'Structural and functional comparison of magnesium transporters throughout evolution', *Cellular and Molecular Life Sciences*, 79(8), p. 418. Available at: https://doi.org/10.1007/s00018-022-04442-8.

Goldberg, R.N., Kishore, N. and Lennen, R.M. (2002) 'Thermodynamic Quantities for the Ionization Reactions of Buffers', *Journal of Physical and Chemical Reference Data*, 31(2), pp. 231–370. Available at: https://doi.org/10.1063/1.1416902.

Grøftehauge, M.K. *et al.* (2015) 'Protein–ligand interactions investigated by thermal shift assays (TSA) and dual polarization interferometry (DPI)', *Acta Crystallographica Section D Biological Crystallography*, 71(1), pp. 36–44. Available at: https://doi.org/10.1107/S1399004714016617.

Groisman, E.A. *et al.* (2013) 'Bacterial Mg^{2+} Homeostasis, Transport, and Virulence', *Annual Review of Genetics*, 47(1), pp. 625–646. Available at: https://doi.org/10.1146/annurev-genet-051313-051025.

Gundlach, J. *et al.* (2019) 'Sustained sensing in potassium homeostasis: Cyclic di-AMP controls potassium uptake by KimA at the levels of expression and activity', *Journal of*

Biological Chemistry, 294(24), pp. 9605–9614. Available at: https://doi.org/10.1074/jbc.RA119.008774.

Hartwig, A. (2001) 'Role of magnesium in genomic stability', *Mutation Research/Fundamental and Molecular Mechanisms of Mutagenesis*, 475(1–2), pp. 113–121. Available at: https://doi.org/10.1016/S0027-5107(01)00074-4.

Hattori, M. *et al.* (2007) 'Crystal structure of the MgtE Mg2+ transporter', *Nature*, 448(7157), pp. 1072–1075. Available at: https://doi.org/10.1038/nature06093.

Hattori, M. *et al.* (2009) 'Mg2+-dependent gating of bacterial MgtE channel underlies Mg2+ homeostasis', *The EMBO Journal*, 28(22), pp. 3602–3612. Available at: https://doi.org/10.1038/emboj.2009.288.

Ignoul, S. and Eggermont, J. (2005) 'CBS domains: structure, function, and pathology in human proteins', *American Journal of Physiology-Cell Physiology*, 289(6), pp. C1369–C1378. Available at: https://doi.org/10.1152/ajpcell.00282.2005.

Jin, F., Huang, Y. and Hattori, M. (2022) 'Recent Advances in the Structural Biology of Mg2+ Channels and Transporters', *Journal of Molecular Biology*, 434(19), p. 167729. Available at: https://doi.org/10.1016/j.jmb.2022.167729.

Leavitt, S. and Freire, E. (2001) 'Direct measurement of protein binding energetics by isothermal titration calorimetry', *Current Opinion in Structural Biology*, 11(5), pp. 560–566. Available at: https://doi.org/10.1016/S0959-440X(00)00248-7.

Maguire, M.E. and Cowan, J.A. (2002) 'Magnesium chemistry and biochemistry', *BioMetals*, 15(3), pp. 203–210. Available at: https://doi.org/10.1023/A:1016058229972.

Marta Maria Noutel Lorga Gomes (2020) *Biochemical and structural characterization of a potassium transporter from Bacillus subtilis*. Mestrado. Universidade do Porto.

Mehne, F.M.P. *et al.* (2013) 'Cyclic Di-AMP Homeostasis in Bacillus subtilis', *Journal of Biological Chemistry*, 288(3), pp. 2004–2017. Available at: https://doi.org/10.1074/jbc.M112.395491.

Moncrief, M.B.C. and Maguire, M.E. (1999) 'Magnesium transport in prokaryotes', *JBIC Journal of Biological Inorganic Chemistry*, 4(5), pp. 523–527. Available at: https://doi.org/10.1007/s007750050374.

Moomaw, A.S. and Maguire, M.E. (2008) 'The Unique Nature of Mg^{2+} Channels', *Physiology*, 23(5), pp. 275–285. Available at: https://doi.org/10.1152/physiol.00019.2008.

Mudgal, S. *et al.* (2021) 'Cyclic di-AMP: Small molecule with big roles in bacteria', *Microbial Pathogenesis*, 161, p. 105264. Available at: https://doi.org/10.1016/j.micpath.2021.105264.

Oppenheimer-Shaanan, Y. *et al.* (2011) 'c-di-AMP reports DNA integrity during sporulation in *Bacillus subtilis*', *EMBO reports*, 12(6), pp. 594–601. Available at: https://doi.org/10.1038/embor.2011.77.

Rude, R.K. (1998) ‘Magnesium Deficiency: A Cause of Heterogenous Disease in Humans’, *Journal of Bone and Mineral Research*, 13(4), pp. 749–758. Available at: https://doi.org/10.1359/jbmr.1998.13.4.749.

Srivastava, V.K. and Yadav, R. (2019) ‘Isothermal titration calorimetry’, in *Data Processing Handbook for Complex Biological Data Sources*. Elsevier, pp. 125–137. Available at: https://doi.org/10.1016/B978-0-12-816548-5.00009-5.

Stülke, J. and Krüger, L. (2020) ‘Cyclic di-AMP Signaling in Bacteria’, *Annual Review of Microbiology*, 74(1), pp. 159–179. Available at: https://doi.org/10.1146/annurev-micro-020518-115943.

Tomita, A. *et al.* (2017) ‘ATP-dependent modulation of MgtE in Mg2+ homeostasis’, *Nature Communications*, 8(1), p. 148. Available at: https://doi.org/10.1038/s41467-017-00082-w.

Vieira-Pires, R.S., Szollosi, A. and Morais-Cabral, J.H. (2013) ‘The structure of the KtrAB potassium transporter’, *Nature*, 496(7445), pp. 323–328. Available at: https://doi.org/10.1038/nature12055.

Wendel, B.M. *et al.* (2022) ‘A Central Role for Magnesium Homeostasis during Adaptation to Osmotic Stress’, *mBio*. Edited by M.S. Turner, 13(1), pp. e00092-22. Available at: https://doi.org/10.1128/mbio.00092-22.

Yin, W. *et al.* (2020) ‘A decade of research on the second messenger c-di-AMP’, *FEMS Microbiology Reviews*, 44(6), pp. 701–724. Available at: https://doi.org/10.1093/femsre/fuaa019.

APPENDIX

Scheme 1– Differential Scanning Fluorimetry plate setup.

MgtE CBS-L and KtrA are present in 5 μM and 10 μM concentrations, in buffer containing different concentrations of SYPRO Orange from two stocks, along with 0 or 1 mM of ATP.

5x SYPRO Orange Stock A		10x SYPRO Orange Stock A		5x SYPRO Orange Stock B		10x SYPRO Orange Stock B	
5μ M KtrA 1mM ATP	5μ M KtrA 1mM ATP	5μ M KtrA 1mM ATP	5μ M KtrA 1mM ATP	5μ M KtrA 1mM ATP	5μ M KtrA 1mM ATP	5μ M KtrA 1mM ATP	5μ M KtrA 1mM ATP
10μ M KtrA 1mM ATP	10μ M KtrA 1mM ATP	10μ M KtrA 1mM ATP	10μ M KtrA 1mM ATP	10μ M KtrA 1mM ATP	10μ M KtrA 1mM ATP	10μ M KtrA 1mM ATP	10μ M KtrA 1mM ATP
5μ M MgtE CBS-L 0mM ATP	5μ M MgtE CBS-L 0mM ATP	5μ M MgtE CBS-L 0mM ATP	5μ M MgtE CBS-L 0mM ATP	5μ M MgtE CBS-L 0mM ATP	5μ M MgtE CBS-L 0mM ATP	5μ M MgtE CBS-L 0mM ATP	5μ M MgtE CBS-L 0mM ATP
10μ M MgtE CBS-L 0mM ATP	10μ M MgtE CBS-L 0mM ATP	10μ M MgtE CBS-L 0mM ATP	10μ M MgtE CBS-L 0mM ATP	10μ M MgtE CBS-L 0mM ATP	10μ M MgtE CBS-L 0mM ATP	10μ M MgtE CBS-L 0mM ATP	10μ M MgtE CBS-L 0mM ATP
5μ M MgtE CBS-L 1mM ATP	5μ M MgtE CBS-L 1mM ATP	5μ M MgtE CBS-L 1mM ATP	5μ M MgtE CBS-L 1mM ATP	5μ M MgtE CBS-L 1mM ATP	5μ M MgtE CBS-L 1mM ATP	5μ M MgtE CBS-L 1mM ATP	5μ M MgtE CBS-L 1mM ATP
10μ M MgtE CBS-L 1mM ATP	10μ M MgtE CBS-L 1mM ATP	10μ M MgtE CBS-L 1mM ATP	10μ M MgtE CBS-L 1mM ATP	10μ M MgtE CBS-L 1mM ATP	10μ M MgtE CBS-L 1mM ATP	10μ M MgtE CBS-L 1mM ATP	10μ M MgtE CBS-L 1mM ATP
empty	empty	Empty	empty	empty	empty	empty	empty

Scheme 2– Differential Scanning Fluorimetry plate setup for follow-up assay.

MgtE CBS-L and CBS-S present in 0 or 10 μM concentration, with 0.5mM of several ligands (DSMO, c-di-AMP, pppgpp, pApA, ci-di-GMP, ppgpp), in buffer containing SYPRO Orange (10x) and presence or absence of Mg^{2+} (10 mM).

empty	empty	empty	empty	empty	empty	empty	empty	empty	empty	empty	empty

CBS-L	CBS-L	CBS-L	CBS-S	CBS-S	CBS-S	CBS-L Mg^{2+}	CBS-L Mg^{2+}	CBS-L Mg^{2+}	CBS-S Mg^{2+}	CBS-S Mg^{2+}	CBS-S Mg^{2+}
CBS-L DMSO	CBS-L DMSO	CBS-L DMSO	CBS-S DMSO	CBS-S DMSO	CBS-S DMSO	CBS-L Mg^{2+} DMSO	CBS-L Mg^{2+} DMSO	CBS-L Mg^{2+} DMSO	CBS-S Mg^{2+} DMSO	CBS-S Mg^{2+} DMSO	CBS-S Mg^{2+} DMSO
CBS-L c-di-AMP	CBS-L c-di-AMP	CBS-L c-di-AMP	CBS-S c-di-AMP	CBS-S c-di-AMP	CBS-S c-di-AMP	CBS-L Mg^{2+} c-di-AMP	CBS-L Mg^{2+} c-di-AMP	CBS-L Mg^{2+} c-di-AMP	CBS-S Mg^{2+} c-di-AMP	CBS-S Mg^{2+} c-di-AMP	CBS-S Mg^{2+} c-di-AMP
CBS-L pppgpp	CBS-L pppgpp	CBS-L pppgpp	CBS-S pppgpp	CBS-S pppgpp	CBS-S pppgpp	CBS-L Mg^{2+} pppgpp	CBS-L Mg^{2+} pppgpp	CBS-L Mg^{2+} pppgpp	CBS-S Mg^{2+} pppgpp	CBS-S Mg^{2+} pppgpp	CBS-S Mg^{2+} Pppgpp
CBS-L pApA	CBS-L pApA	CBS-L pApA	CBS-S pApA	CBS-S pApA	CBS-S pApA	CBS-L Mg^{2+} pApA	CBS-L Mg^{2+} pApA	CBS-L Mg^{2+} pApA	CBS-S Mg^{2+} pApA	CBS-L Mg^{2+} pApA	CBS-S Mg^{2+} PApA
CBS-L c-di-GMP	CBS-L c-di-GMP	CBS-L c-di-GMP	CBS-S c-di-GMP	CBS-S c-di-GMP	CBS-S c-di-GMP	CBS-L Mg^{2+} c-di-GMP	CBS-L Mg^{2+} c-di-GMP	CBS-L Mg^{2+} c-di-GMP	CBS-S Mg^{2+} c-di-GMP	CBS-S Mg^{2+} c-di-GMP	CBS-S Mg^{2+} c-di-GMP
CBS-L ppgpp	CBS-L ppgpp	CBS-L ppgpp	CBS-S ppgpp	CBS-S ppgpp	CBS-S ppgpp	CBS-L Mg^{2+} ppgpp	CBS-L Mg^{2+} ppgpp	CBS-L Mg^{2+} ppgpp	CBS-S Mg^{2+} ppgpp	CBS-S Mg^{2+} ppgpp	CBS-S Mg^{2+} ppgpp

Scheme 3– Reservoir composition of follow-up optimization 48-well plate for MgtE CBS-S crystallization.

All wells contain Buffer System 2 (see below) pH 7.5 and varying concentrations of Precipitant Mix 2 (v/v, PM2). Half the wells contain 0.1 M Carboxylic Acids Mix (CA), shown in blue, and the others contain 0.9 M NPS Mix (NPS), shown in red. Composition of mixes (see below) were as described by the manufacturer of Morpheus crystallization screen.

CA 22% PM2 0mM Mg^{2+}	CA 22% PM2 0.5mM Mg^{2+}	CA 22% PM2 1mM Mg^{2+}	NPS 22% PM2 0mM Mg^{2+}	NPS 22% PM2 0.5mM Mg^{2+}	NPS 22% PM2 1mM Mg^{2+}
CA 24% PM2 0mM Mg^{2+}	CA 24% PM2 0.5mM Mg^{2+}	CA 24% PM2 1mM Mg^{2+}	NPS 24% PM2 0mM Mg^{2+}	NPS 24% PM2 0.5mM Mg^{2+}	NPS 24% PM2 1mM Mg^{2+}
CA 26% PM2 0mM Mg^{2+}	CA 26% PM2 0.5mM Mg^{2+}	CA 26% PM2 1mM Mg^{2+}	NPS 26% PM2 0mM Mg^{2+}	NPS 26% PM2 0.5mM Mg^{2+}	NPS 26% PM2 1mM Mg^{2+}
CA 28% PM2 0mM Mg^{2+}	CA 28% PM2 0.5mM Mg^{2+}	CA 28% PM2 1mM Mg^{2+}	NPS 28% PM2 0mM Mg^{2+}	NPS 28% PM2 0.5mM Mg^{2+}	NPS 28% PM2 1mM Mg^{2+}

CA 30% PM2 0mM Mg^{2+}	CA 30% PM2 0.5mM Mg^{2+}	CA 30% PM2 1mM Mg^{2+}	NPS 30% PM2 0mM Mg^{2+}	NPS 30% PM2 0.5mM Mg^{2+}	NPS 30% PM2 1mM Mg^{2+}
CA 32% PM2 0mM Mg^{2+}	CA 32% PM2 0.5mM Mg^{2+}	CA 32% PM2 1mM Mg^{2+}	NPS 32% PM2 0mM Mg^{2+}	NPS 32% PM2 0.5mM Mg^{2+}	NPS 32% PM2 1mM Mg^{2+}
CA 34% PM2 0mM Mg^{2+}	CA 34% PM2 0.5mM Mg^{2+}	CA 34% PM2 1mM Mg^{2+}	NPS 34% PM2 0mM Mg^{2+}	NPS 34% PM2 0.5mM Mg^{2+}	NPS 34% PM2 1mM Mg^{2+}
CA 36% PM2 0mM Mg^{2+}	CA 36% PM2 0.5mM Mg^{2+}	CA 36% PM2 1mM Mg^{2+}	NPS 36% PM2 0mM Mg^{2+}	NPS 36% PM2 0.5mM Mg^{2+}	NPS 36% PM2 1mM Mg^{2+}